Dual-domain Flower signaling coordinates extracellular vesicles-mediated fitness selection and cell-intrinsic survival in astrocytes

Running title: Flower EVs regulate astrocyte fitness

Szu-Min Tu[1,2], Ching-Hsin Lin[1,2], Yang Liu[2,3], Claudia Schirra[1,2], Chin-An Yang[4,5], Johannes Hohneck[6], Martin Jung[7], Annika Clemenz[8], Sandra Rother[8], Ahmad Aljohmani[9], Daniela Yildiz[9], Yvonne Schwarz[10], Elmar Krause[1], Walter J. Schulz-Schaeffer[11], Veit Flockerzi[12], Chi-Kuang Yao[13,14], Hsin-Fang Chang*[1,2,15]

1. Cellular Neurophysiology, Center for Integrative Physiology and Molecular Medicine (CIPMM), Saarland University, 66421 Homburg, Germany
2. Center for Gender-specific Biology and Medicine (CGBM), University of Saarland, 66421 Homburg, Germany
3. Department of Neurology, Saarland University, 66421 Homburg, Germany
4. Integrated Precision Health and Immunodiagnostic Center, Department of Laboratory Medicine, China Medical University Hsinchu Hospital, Zhubei City, Taiwan
5. Department of Laboratory Medicine, Chang Gung Memorial Hospital, Linkou, Taiwan
6. Department of Pathology, Saarland University, 66421 Homburg, Germany
7. Medical Biochemistry and Molecular Biology, Saarland University, 66421 Homburg, Germany.
8. Biophysics, Center for Integrative Physiology and Molecular Medicine (CIPMM), Saarland University, 66421 Homburg, Germany
9. Molecular Pharmacology, PZMS, Saarland University, Campus Homburg Building 46, 66421, Homburg, Germany.
10. Institute for Physiology, Center of Integrative Physiology and Molecular Medicine (CIPMM), Saarland University, Homburg, Germany.
11. Institute for Neuropathology, Medical Faculty, Saarland University, 66421 Homburg, Germany
12. Experimental and Clinical Pharmacology and Toxicology, Saarland University, Building 46, 66421 Homburg, Germany.
13. Neuroscience Program of Academia Sinica, Academia Sinica, Taipei, Taiwan
14. Institute of Biochemical Sciences, College of Life Science, National Taiwan University, Taipei, Taiwan
15. Department of Medicinal and Applied Chemistry, Kaohsiung Medical University, 100 Shih-Chuan 1st Road, 80708 Kaohsiung, Taiwan

* Correspondence:
Dr. Hsin-Fang Chang
Cellular Neurophysiology, CIPMM, Saarland University
66421 Homburg, Germany
T: +49 (0) 6841 16 16400
Email: Hsin-Fang.Chang@uks.eu

Abstract

Cellular fitness surveillance preserves tissue integrity, yet its regulation within the mammalian brain remains poorly understood. We identify a bifurcated mechanism in the transmembrane protein Flower—encoding both survival-promoting (“win”) and apoptosis-inducing (“lose”) isoforms. We demonstrate that astrocytes secrete specialized extracellular vesicles (EVs), termed “fitness vesicles,” carrying Flower to facilitate competitive selection across distal cell populations. The N-terminal Flower domain acts extrinsically via these EVs to drive the elimination of less-fit neighbors. Conversely, the "win"-specific C-terminal domain functions as a cell-intrinsic module; it translocates to the nucleus under stress to repress Caspase-3 and provide resilience. In Alzheimer’s disease (AD) models and human AD brains, Flower-positive astrocytes accumulate around amyloid-β (Aβ) plaques. Under Aβ stress, the “win” isoform reprograms astrocytes toward a neuroprotective state that enhances plaque clearance while ensuring cell-intrinsic survival. Our findings reveal how Flower couples long-range, EV-mediated cellular selection with cell-autonomous protection to coordinate astrocyte quality control and tissue resilience in neurodegeneration.

INTRODUCTION

Intercellular communication is fundamental to brain homeostasis and occurs through both direct cell–cell contact and secreted extracellular vesicles (EVs)(Schnatz *et al*, 2021). Astrocyte-derived EVs modulate synaptic activity, inflammatory responses, and amyloid-β (Aβ) metabolism, underscoring their role in neural tissue regulation(Chaudhuri *et al*, 2018; Li *et al*, 2020b; Patel & Weaver, 2021; You *et al*, 2020). However, whether EV-mediated communication contributes to cellular fitness surveillance in the mammalian brain remains unknown. In particular, it is unclear whether molecular determinants of cellular fitness, conventionally viewed as mediators of contact-dependent competition, can be transmitted via EVs to regulate competitive cellular outcomes across extended distances beyond direct membrane contact.

The transmembrane protein Flower was first identified in *Drosophila melanogaster* as a regulator of synaptic vesicle endocytosis (Yao *et al*, 2009). Subsequent studies have confirmed Flower's role in endocytosis in both invertebrates and vertebrates(Chang *et al*, 2018; Ravichandran *et al*, 2024; Xue *et al*, 2012; Yao *et al.*, 2009; Yao *et al*, 2017). *Flower* is evolutionarily conserved from flies to mammals and is ubiquitously expressed across tissues, highlighting its ancient and essential biological functions. The gene encodes multiple isoforms, some of which are involved in calcium channel activity and vesicle trafficking(Brose & Neher, 2009; Kuo & Trussell, 2009; Li *et al*, 2020a; Seidenthal *et al*, 2025; Yao *et al.*, 2009; Yao *et al.*, 2017). More recently, specific Flower isoforms have been recognized as key regulators of a fundamental process known as cellular fitness competition(Merino *et al*, 2013; Rhiner *et al*, 2010), a natural selection mechanism that eliminates unfit cells by inducing apoptosis while allowing healthy, fit cells to continue growing(Madan *et al*, 2018; Merino *et al*, 2016; Merino *et al*, 2015). This selection process results in the survival of fitter ‘winner’ cells, while unfit ‘losers’ are eliminated from the population.

In heterogeneous cell populations, Flower isoforms function as molecular "fitness fingerprints" displayed on the cell surface(Merino *et al.*, 2013; Rhiner *et al.*, 2010). Fit cells predominantly express “win” isoforms, while less-fit cells express “lose” isoforms. This differential expression drives selective apoptosis of unfit cells and survival of fitter neighbors, establishing a winner–loser signaling axis. Such fitness-based cell selection is essential for tissue integrity during embryonic development, aging, infection, tumorigenesis, and neurodegeneration(Coelho & Moreno, 2019; Costa-Rodrigues *et al*, 2021; Gogna *et al*, 2015; Madan *et al*, 2020; Madan *et al*, 2019; Marques-Reis & Moreno, 2021; Parker *et al*, 2020; Yekelchyk *et al*, 2021). Despite its broad relevance, the mechanistic basis of Flower-mediated signaling in mammals remains poorly understood.

Tissue homeostasis depends on maintaining a balanced fitness landscape. Neurodegenerative conditions disrupt this equilibrium, generating heterogeneous cell populations with divergent survival capacities. Astrocytes are central regulators of brain homeostasis and play key roles in Aβ clearance and neuronal support in Alzheimer’s disease (AD)(Dai *et al*, 2023; Gomez-Arboledas *et al*, 2018; Jiwaji *et al*, 2022; Kim *et al*, 2022; Lines *et al*, 2022). However, astrocytic responses are highly heterogeneous(Moonen *et al*, 2023; Patani *et al*, 2023), suggesting the presence of intrinsic selection mechanisms that influence cell survival and function. Whether Flower-mediated fitness signaling contributes to this heterogeneity remains unknown.

Here, we present experimental evidence that points the existing model of Flower-mediated signaling in a new direction. Our topological analyses demonstrate that in intact astrocytes, both the N- and C-terminal signaling domains of Flower are localized in the cytoplasm, rendering them sequestered from direct intercellular contact. To resolve this paradox, we identify a novel extracellular vesicle (EV)–associated pathway that serves as the essential vehicle for signal presentation. We show that incorporation into specialized “fitness vesicles” triggers a topological transition, exposing these domains to the extracellular environment and enabling long-range intercellular selection across distal cell populations. Using complementary molecular and imaging approaches, we define the functional roles of this mechanism under Aβ stress, validating our findings in APP-transgenic mice and human Alzheimer’s disease tissue. Together, our results uncover a previously unrecognized dual-domain mechanism that bifurcates Flower signaling into EV-mediated distal selection and cell-intrinsic protection, providing a new model for understanding tissue resilience in neurodegeneration.

RESULTS

Flower isoforms mediate differential cell survival in primary astrocytes

Flower is a conserved cell fitness marker that labels cells as “winners” or “losers” during competitive interactions. In mice, the Flower locus encodes four isoforms (Fig. 1A), of which mFwe2 and mFwe4 are associated with a “win” phenotype, whereas mFwe1 and mFwe3 confer a “lose” identity(Petrova *et al*, 2012). To investigate how Flower isoforms regulate astrocyte fitness, we established a quantitative cell competition assay using primary astrocytes derived from Flower knockout (KO) mice.

Specific Flower isoforms were reintroduced into KO astrocytes by electroporation to generate defined winner and loser populations. Astrocytes expressing individual isoforms were then co-cultured in pairwise combinations, including homotypic (mFwe1 + mFwe1, mFwe2 + mFwe2, mFwe3 + mFwe3) and heterotypic (mFwe1 + mFwe2, mFwe1 + mFwe3, mFwe1 + mFwe4, mFwe2 + mFwe1, mFwe2 + mFwe3, mFwe2 + mFwe4, mFwe3 + mFwe4) conditions, enabling classification into win–win, lose–lose, and win–lose interactions (Fig. 1B).

After 24 h of co-culture, dynamic interactions were observed, particularly in heterotypic pairings, characterized by cell–cell contact and selective cell elimination. Cell death was assessed using two complementary approaches: pre-fixation application of the membrane-impermeable dye DAPI to label cells with compromised membrane integrity, and post-fixation immunostaining for cleaved caspase-3 (CC3) to detect apoptosis (Fig. 1C). Cell–cell contact pairs were analyzed to determine viability, with dead cells classified as either early apoptotic ($CC3^+$) or late apoptotic/necrotic ($DAPI^+$ with nuclear fragmentation).

In win–win and lose–lose homotypic cultures, overall cell death remained low (6–8%). In contrast, heterotypic co-cultures of win and lose isoforms exhibited a marked increase in apoptosis, with approximately 45% of cells undergoing cell death (Fig. 1D). Notably, apoptosis occurred predominantly in cells expressing the lose isoforms. In the Fwe1 + Fwe2, Fwe2 + Fwe3, Fwe3 + Fwe4, and Fwe1 + Fwe4 co-cultures, cells expressing either mFwe1 or mFwe3 were consistently eliminated, confirming their functional identity as “loser” isoforms. Overall, 35–45% of less-fit astrocytes were selectively removed through Flower-mediated cell competition (Fig. 1E).

To determine whether this fitness code is conserved across species, we next tested the human Flower isoforms hFWE3 (“lose”) and hFWE4 (“win”), whose phenotypes have been previously characterized in tumor models(Madan *et al.*, 2019). As in the mouse system, homotypic win–win (hFWE4 + hFWE4) and lose–lose (hFWE3 + hFWE3) cultures showed minimal cell death. In contrast, co-culture of hFWE3- and hFWE4-expressing astrocytes resulted in ~40% total cell death within the mixed population (Fig. 1F,G), with selective elimination of ~40% of hFWE3-expressing cells (Fig. 1H).

Together, these results establish a robust primary astrocyte co-culture system that faithfully recapitulates Flower-dependent elimination of less-fit cells by fitter neighbors. This assay provides a quantitative platform for dissecting the molecular mechanisms and signaling domains underlying Flower-mediated fitness surveillance in glial cells.

144

145 **N- and C-termini of Flower isoforms localize to the cytoplasmic side in astrocytes**

146 Cellular fitness is generally considered to be regulated via cell–cell contact(Rhiner *et al.*, 2010), implying
147 that the functional domains of Flower isoforms should be exposed on the cell surface. However,
148 topological predictions for full-length mouse Flower isoforms are inconsistent with experimental
149 observations(Chang *et al.*, 2018; Petrova *et al.*, 2012). To address this discrepancy, we first examined
150 the expression of all Flower isoforms in primary mouse astrocytes by quantitative RT-PCR. All four
151 mouse Flower isoforms were detected, with mFwe1 and mFwe2 representing the predominant lose and
152 win isoforms, respectively (Fig. 2A). Based on their relative abundance and established functional
153 relevance, we subsequently focused our topological analyses on mFwe1 (lose) and mFwe2 (win).

154 Super-resolution SIM revealed that both Flag/HA tagged mFwe1- and mFwe2-expressing WT
155 astrocytes displayed a punctate intracellular distribution, with partial localization at the plasma
156 membrane, consistent with Flower being a vesicular membrane protein (Ravichandran *et al.*, 2024; Yao
157 *et al.*, 2009) (Fig. 2B). To determine the topology of Flower isoforms, we fused the pH-sensitive GFP
158 variant pHluorin2 to either the N- or C-terminus of mFwe1 and mFwe2. Primary astrocytes were
159 transfected with these constructs and subjected to live-cell confocal imaging to monitor ratiometric
160 fluorescence (405/488 nm) following cytosolic acidification induced by the protonophore carbonyl
161 cyanide m-chlorophenyl hydrazone (CCCP). Astrocytes were maintained in DMEM during imaging, and
162 DMSO-treated cells served as vehicle controls. Cytosolic pHluorin2 and vesicle-luminal
163 Synaptobrevin2–pHluorin2 (Syb2-pHluorin2) were included as localization controls.

164 CCCP treatment induced a robust decrease in the 405/488 fluorescence ratio in cells expressing
165 cytosolic pHluorin2, confirming effective cytoplasmic acidification (Fig. 2C). Both N- and C-terminally
166 tagged mFwe1 constructs exhibited comparable decreases in fluorescence ratio (Fig. 2D,E), indicating
167 cytoplasmic exposure of both termini. In contrast, vesicle-luminal Syb2-pHluorin2 remained unchanged
168 despite robust cytosolic acidification (Fig. 2F), demonstrating that pHluorin2 confined to intracellular
169 lumens is not responsive to CCCP-induced cytoplasmic pH shifts. Similarly, mFwe2 constructs tagged
170 at either terminus displayed comparable decreases in fluorescence ratio upon CCCP treatment (Fig.
171 2G,H), indicating that both termini of mFwe2 are likewise cytoplasmic.

172 Because luminally oriented pHluorin2 does not respond to cytosolic acidification in this assay, Flower
173 molecules with an inward-facing orientation would not contribute to the measured 405/488 ratio. The
174 ratiometric signal therefore reflects the predominant cytoplasmic exposure of the tagged termini.
175 Although the presence of a minor pool of Flower proteins with alternative orientation or subcellular
176 localization cannot be excluded, the data indicate that the majority of both N- and C-termini of mFwe1
177 and mFwe2 are cytoplasmically exposed in astrocytes.

178 Together, these results establish that both the majority of lose isoform mFwe1 and the win isoform
179 mFwe2 possess cytoplasmic N- and C-terminal domains in astrocytes. This topology challenges the
180 prevailing model of Flower-mediated fitness regulation as a strictly contact-dependent process(Rhiner

181 *et al.*, 2010) and suggests that Flower may operate through an alternative, non–cell-autonomous
182 signaling mechanism in astrocytes.

183

184 **Flower is released on extracellular vesicles to mediate fitness competition**

185 In *Drosophila*, Flower-mediated fitness recognition relies on extracellular exposure of the C-terminal
186 domain, enabling contact-dependent signaling between neighboring cells(Rhiner *et al.*, 2010). In
187 contrast, our topological analyses demonstrate that both N- and C-termini of Flower isoforms are
188 oriented toward the cytoplasm in astrocytes, suggesting an alternative, non–cell-autonomous
189 mechanism of signaling. To distinguish total Flower protein from isoform-specific C-terminal exposure,
190 we employed two complementary antibodies: a polyclonal Pan-Flower antibody, raised against
191 conserved regions and recognizing both mouse and human Flower proteins without distinguishing
192 isoforms, and a custom C-terminal-specific antibody (#C1557) that selectively detects mouse win
193 isoforms (mFwe2 and mFwe4) but recognizes both hFWE3 and hFWE4 in human tissue.

194 Consistent with the possibility of extracellular Flower, immunoreactivity detected with the #C1557
195 antibody was frequently observed plaque-adjacent regions in brain tissue from both APP-transgenic
196 mice and Alzheimer's disease patients (Fig. EV1A). While this extracellular signal did not overlap with
197 astrocytic markers, its proximity to plaques suggests a secreted pool of Flower, potentially associated
198 with EVs or amyloid-bound assemblies. To investigate the mechanism of release, we analyzed Flower
199 processing in Flower KO astrocytes overexpressing Flag-Flower-HA constructs. Western blot analysis
200 revealed the presence of both full-length Flower and lower molecular weight fragments detected by
201 anti-Flag (N-terminal) and anti-HA (C-terminal) antibodies, consistent with partial proteolytic processing.
202 Quantification was performed based on band intensity integration of full-length and cleaved fragments.
203 Bands corresponding to lower molecular weight species within the same lane were considered
204 processed forms. The win isoform mFwe2 exhibited substantial processing, with approximately 40%
205 full-length protein and ~60% cleaved fragments, whereas other isoforms remained predominantly full-
206 length (70–80%) (Fig. EV1B–D).

207 We next asked whether Flower fragments are secreted via EVs. EVs were isolated from astrocyte
208 culture supernatants by differential ultracentrifugation, with a final pelleting step at 100,000 × g. Western
209 blot analysis of purified EV fractions from WT, mFwe1-, and mFwe2-overexpressing astrocytes showed
210 CD63 enrichment, confirming existence of EV population (Fig. 3A). Immunostaining with the Pan-Flower
211 antibody revealed Flower-positive puncta in supernatants from both WT and mFwe2-pHluorin2-
212 expressing astrocytes (Fig. EV2A). SIM imaging showed that approximately 20% of these puncta co-
213 localized with the membrane dye DiD, whereas ~80% did not. This suggests that a majority of secreted
214 Flower exists either in small, low-lipid vesicles below the DiD labeling threshold or as non-membranous
215 protein-RNA/lipid complexes (Fig. EV2B).

216 To assess isoform-specific secretion, we analyzed supernatants from astrocytes expressing either the
217 win isoform mFwe2 or the lose isoform mFwe1, each tagged with Flag and HA at the N- and C-termini,
218 respectively (Fig. 3B). SIM imaging of supernatants from astrocytes expressing N- and C-terminally

219 tagged mFwe1 or mFwe2 revealed double-positive ($Flag^+/HA^+$) as well as single-positive puncta. These
220 observations indicate the presence of Flower isoforms containing both termini, as well as puncta
221 associated with isolated N- or C-terminal domains (Fig. EV2C). Particle size analysis showed
222 comparable EV radii across conditions (mean radius: 71.6 nm for GFP control, 74.9 nm for mFwe1, and
223 76.0 nm for mFwe2; Fig. EV2D). In this experiment, mFwe1-expressing astrocytes released 3.7×10^7
224 particles per million cells, while mFwe2-expressing cells released 1.6×10^7 particles per million cells,
225 indicating detectable EV secretion from both isoforms.

226 Transmission electron microscopy (TEM) combined with immunogold labeling provided direct
227 ultrastructural evidence that Flower is present on secreted EVs. In WT astrocyte-derived EVs, 10 nm
228 gold particles conjugated to the Pan-Flower antibody were detected on the surface of morphologically
229 intact vesicles (Fig. 3C), establishing extracellular localization of endogenous Flower. In EVs derived
230 from Flag-mFwe2-HA–expressing astrocytes, both 6 nm (Flag) and 10 nm (HA) gold particles were
231 detected on single vesicles (Fig. 3D), demonstrating that full-length mFwe2 is incorporated into EV
232 membranes with extracellular exposure of both termini. Controls without primary antibody showed
233 minimal background (Fig. EV2E). Across conditions, EVs carried an average of ~2 Flower molecules
234 per vesicle, with mean diameters of ~65 nm for WT EVs and ~83 nm for mFwe2-overexpressing EVs
235 (Fig. 3E,F).

236 Western blot analysis of purified EV fractions confirmed the incorporation of mFwe1 and mFwe2 into
237 EVs, as detected by anti-Flag, anti-HA, and Pan-Flower antibodies. The absence of GAPDH in the EV
238 fractions confirmed the purity of the preparation and the absence of cellular debris (Fig. 3G; Fig. EV2F).
239 Despite equal loading (10 μg EV protein), endogenous Flower was below detection level, whereas
240 mFwe2 consistently produced strong signals. Blots were initially probed with anti-Flower, then stripped
241 and sequentially reprobed with anti-HA and anti-Flag antibodies. For quantitative comparison of
242 isoform-specific secretion into EVs, anti-Flag signals were used because they exhibited high specificity
243 and a linear detection range under the experimental conditions. Signal intensities were normalized to
244 the number of transfected cells. Astrocytes expressing mFwe2 secreted ~25-fold more Flower into EVs
245 than those expressing mFwe1, revealing pronounced isoform-specific differences in EV release (Fig.
246 3H). Notably, although mFwe1-overexpressing cells produced more particles than mFwe2-expressing
247 cells, the total Flower protein carried by mFwe2-derived EVs was substantially higher. Differences in
248 transfection efficiency were modest (51% for mFwe2 vs. 42% for mFwe1), and mean fluorescence
249 intensity per cell was comparable, indicating similar expression levels on a per-cell basis (Fig. EV2G,H).

250 Finally, we assessed the functional capacity of these vesicles to execute fitness selection. Treatment of
251 'unfit' (mFwe1-expressing) astrocytes with EVs purified from mFwe2-expressing cells induced robust
252 apoptosis (>30%), whereas WT or mFwe1-derived EVs failed to elicit a death response (Fig. 3I,J).
253 These data establish that EV-associated mFwe2 is a functionally potent effector of fitness competition.
254 Together, our results uncover a non–cell-autonomous mechanism of Flower signaling that is
255 fundamentally distinct from the classical contact-dependent model, providing a framework for long-
256 range fitness surveillance in the mammalian brain.

257

258 **Flower is secreted via a non-canonical, CD63-independent vesicle population**

259 To characterize the biogenesis of Flower-positive EVs, we compared their molecular signature to
260 canonical exosomes using a topologically-defined CD63-pHuji reporter (Verweij *et al*, 2018).
261 Intracellular analysis in astrocytes revealed that both Flower isoforms (mFwe1 and mFwe2) showed
262 minimal co-localization with CD63-positive multivesicular bodies (MVBs) (Fig. EV3A,B). This suggests
263 that the Flower protein bypasses the classical endosomal sorting pathway.

264 Super-resolution SIM imaging and ultrastructural analysis of isolated EVs from mFwe2 overexpressed
265 astrocytes confirmed that Flower and CD63 reside in largely distinct vesicle populations. While a minor
266 fraction (up to 15%) of $CD63^+$ exosomes contained sequestered Flower within their lumen, the vast
267 majority (~70%) of Flower-positive puncta were CD63-negative (Fig. EV3C,D). Immunogold TEM
268 further demonstrated that on these CD63-negative vesicles, both the N- and C-termini of Flower are
269 exposed on the external surface (Fig. EV3E,F). The specificity of this labeling was confirmed using
270 secondary-antibody-only controls, which showed minimal gold particle background (Fig. EV3G).

271 This "extracellular-out" topology is incompatible with the inward budding mechanism of MVB-derived
272 exosomes, which would instead sequester the termini inside the vesicle lumen. These data establish
273 that Flower is predominantly secreted via a non-canonical pathway, likely involving direct budding or
274 recruitment to the limiting membrane of a specialized vesicle class. Based on their distinct molecular
275 identity, unique topology, and role in fitness signaling, we designate these CD63-independent, Flower-
276 exposing vesicles as "fitness vesicles" (Fig. EV3H).

277

278 **Flower's N-terminus induces apoptosis, whereas its C-terminus antagonizes death signaling**

279 To identify functional regions of Flower involved in fitness signaling, we focused on three domains
280 containing potential interaction motifs: the N-terminus (YxxL)(Liu *et al*, 2012), exon 3 (conferring a win
281 phenotype in human cells)(Madan *et al.*, 2019), and the C-terminus (YxxI)(Cheng *et al*, 2017) (Fig. 4A).
282 Our findings demonstrate that while the N- and C-terminal domains are oriented toward the cytoplasm,
283 they are exposed on the outer membrane of astrocyte-derived EVs. To enrich these signaling domains
284 on the cell surface, we engineered them to face the outer plasma membrane. Given that Flower
285 functions as a fitness code(Rhiner *et al.*, 2010), we hypothesized that these specific domains mediate
286 the intercellular signals regulating survival or apoptosis. To test this, we generated truncated Flower
287 constructs fused to mScarlet I and a platelet-derived growth factor receptor (PDGFR) transmembrane
288 domain (mFwe-mScarlet I-TM), allowing ectopic presentation of individual Flower domains at the
289 plasma membrane (Fig. EV4A). Surface localization of these constructs in astrocytes was confirmed by
290 RFP and HA staining under non-permeabilizing conditions (Fig. EV4B). The constructs were expressed
291 in Flower KO astrocytes, which were then separately co-cultured with either mFwe2-expressing (fit) or
292 mFwe1-expressing (unfit) cells to assess cell death (Fig. 4B).

293 Expression of the N-terminal-TM Flower domain selectively induced apoptosis in unfit cells when co-
294 cultured with fit cells, whereas fit cells remained unaffected (Fig. 4C,D; Fig. EV4C). To determine
295 whether this effect was mediated directly by the Flower peptide rather than by secondary cellular

interactions, we treated cells with synthetic peptides corresponding to the truncated Flower domains (Fig. 4E). Consistent with the co-culture experiments, the synthetic N-terminal peptide induced apoptosis specifically in unfit cells (Fig. 4F). This effect was dose-dependent, with apoptosis reaching approximately 35% at higher peptide concentrations, closely matching the magnitude observed in the cell-based assays (Fig. 4G).

Given that win isoforms of Flower contain a unique C-terminal domain, we next tested whether this region confers resistance to N-terminal-mediated apoptosis. Unfit cells expressing mFwe1 or mFwe3 were co-transfected with a C-terminal-TM construct and exposed to the N-terminal peptide. Expression of the C-terminal domain significantly reduced apoptosis under these conditions (Fig. 4H,I). Importantly, overexpression of the C-terminal domain alone did not enhance basal cell survival (Fig. EV5A,B), indicating that this domain does not actively promote survival but instead antagonizes N-terminal–induced death signaling.

To further define the downstream pathways involved, we analyzed the expression of apoptosis-related genes in unfit cells treated with the N-terminal peptide, with or without C-terminal-TM domain expression. N-terminal peptide treatment induced the upregulation of *Caspase3* and *Bax* mRNA, consistent with activation of the intrinsic apoptotic pathway. Conversely, co-expression of the C-terminal domain suppressed this induction, while *Bcl2* levels remained stable (Fig. 4J). These results demonstrate that Flower-mediated death primarily engages a transcriptional *Bax-Caspase3* axis.

Together, these results demonstrate that Flower's N-terminus triggers apoptosis in unfit astrocytes, whereas the C-terminus counteracts this death signal.

Direct interaction between Flower N- and C-terminal domains modulates pro-apoptotic fitness signaling

Our functional assays (Fig. 4) identified a fundamental dichotomy in Flower signaling: the N-terminal domain triggers apoptosis in "unfit" astrocytes, while the C-terminal domain antagonizes this death signal. Since the N- and C-termini of Flower are cytoplasmically oriented in astrocytes, this suggests that their antagonistic interaction is specifically coordinated upon secretion.

To determine the biochemical basis for this antagonism, we performed Surface Plasmon Resonance (SPR) assays using synthetic peptides. A C-terminal peptide was immobilized on the sensor chip, and N- or C-terminal peptides were injected as analytes. SPR revealed a specific, concentration-dependent interaction between the N- and C-terminal peptides, whereas no self-association was observed for the C-terminal peptide alone (Fig. EV6A,B). Notably, the N-terminal peptide exhibited strong dose-dependent self-association (Fig. EV6C,D), suggesting that it may oligomerize to enhance its pro-apoptotic signaling potency.

These findings provide a biochemical framework for the modular signaling logic of Flower. We propose that the extracellular C-terminal domain attenuates death signaling through direct binding-dependent interference, effectively masking the N-terminal "death ligand"

333 Based on these results, we propose a model for Flower-mediated fitness regulation (Fig. 5). In the
334 intracellular environment, Flower termini are cytoplasmically sequestered. Upon release via "fitness
335 vesicles," the preservation of membrane topology results in an "extracellular-out" orientation, exposing
336 both domains on the EV surface. In this extracellular context, the N-terminal fragment transmits pro-
337 apoptotic signals to promote the elimination of distal unfit cells. However, on "win" (mFwe2) vesicles or
338 target cell surfaces, the C-terminal domain acts as a molecular shield, neutralizing the N-terminal signal
339 through direct physical binding.

340 Consistent with this framework, both "win" (mFwe2) and "lose" (mFwe1) isoforms contain the pro-
341 apoptotic N-terminal region. However, only the mFwe2 isoform includes the C-terminal antagonistic
342 domain, enabling the selective protection of "fit" cells from fitness-induced elimination through this
343 localized, surface-masking mechanism.

344

345 **Localized enrichment of Flower isoforms in astrocytes surrounding amyloid plaques in mouse**
346 **and human Alzheimer's disease brains**

347 To investigate whether Flower-mediated fitness signaling is engaged in human neurodegeneration, we
348 first analyzed the expression of the Flower gene *CACFD1* in hippocampal specimens from patients with
349 Alzheimer's disease (AD) and age-matched healthy controls. Analysis of publicly available microarray
350 data revealed that *CACFD1* expression positively correlates with AD disease severity, including incipient,
351 moderate, and severe stages, as assessed by Braak stage and neurofibrillary tangle (NFT) score
352 (Blalock *et al*, 2004) (Fig. 6A). While control individuals exhibited generally low *CACFD1* expression,
353 transcript levels progressively increased with advancing disease stage. This gradual upregulation
354 resulted in a significant elevation of *CACFD1* expression in severe AD patients compared with healthy
355 donors (Fig. 6B), indicating an association between Flower expression and disease progression in the
356 human brain.

357 To validate these transcriptomic findings at the cellular level, we examined post-mortem cortical tissue
358 from AD patients by immunohistochemistry. Consistent with previous reports, $GFAP^+$ astrocytes
359 accumulated around amyloid plaques(Sanchez-Mico *et al*, 2021). Notably, a subset of these plaque-
360 associated astrocytes—defined as cells located within approximately 50 μm of plaque borders—
361 displayed robust Flower immunoreactivity (Fig. 6C,D). Quantitative analysis revealed that ~45% of
362 astrocytes in plaque-associated regions expressed high levels of Flower, compared with ~7% in non-
363 plaque areas (Fig. 6E). The pronounced enrichment of Flower-positive astrocytes near plaques
364 indicates locally elevated Flower signaling within the plaque microenvironment in human AD brains.

365 To determine whether Flower-mediated fitness signaling is engaged in vivo during neurodegeneration,
366 we analyzed the APP transgenic mouse model of Alzheimer's disease, which develops amyloid plaque
367 pathology. We hypothesized that plaque-associated cortical regions may represent microenvironments
368 of heterogeneous cellular fitness regulated by Flower-dependent signaling. RT–qPCR analysis of total
369 cortical tissue showed no significant difference in overall Flower isoform expression between APP and
370 WT mice (Fig. 6F). To examine spatial regulation, plaque-adjacent and plaque-free cortical regions were

371 isolated using laser capture microdissection following Congo Red staining. Quantitative RT–PCR
372 analysis showed that mFwe2 is the predominant Flower isoform in both plaque-associated and non-
373 plaque cortical regions (Fig. 6G). However, mFwe2 expression was higher in plaque-adjacent regions
374 compared with plaque-free cortical tissue, suggesting spatially restricted regulation of Flower
375 expression during amyloid pathology.

376 To selectively assess Flower win isoform expression in mouse tissue, we performed immunostaining
377 using the win-isoform–specific C-terminal antibody #C1557. As expected, Iba1^{+} microglia and GFAP^{+}
378 astrocytes accumulated around amyloid plaques (Fig. 6G). Co-staining revealed a marked enrichment
379 of Flower win–high astrocytes in the immediate plaque vicinity (Fig. 6H,I), with ~45% of astrocytes near
380 plaques exhibiting high Flower win expression compared with ~7% in distal regions (Fig. 6J). In contrast,
381 Flower win expression was largely absent from microglia, with only ~4% of plaque-associated microglia
382 and ~0.5% of distal microglia displaying detectable Flower win levels (Fig. 6J).

383 Together, these data demonstrate a conserved, spatially restricted upregulation of Flower expression
384 in astrocytes surrounding amyloid plaques in both human and mouse AD brains. The correlation
385 between Flower expression and disease severity, combined with its selective enrichment in plaque-
386 associated astrocytes, supports a model in which Flower-mediated fitness signaling contributes to
387 astrocyte responses and tissue resilience in the neurodegenerative microenvironment.

388

389 **Flower win signaling enhances astrocytic Aβ uptake and protects neurons under amyloid stress**

390 To determine whether Flower-mediated fitness signaling is functionally engaged during amyloid-induced
391 neurodegeneration, we established an amyloidogenic neuron–glia co-culture model that recapitulates
392 key aspects of Aβ accumulation and cytotoxicity. Primary cortical cultures were exposed to Aβ42
393 protofibrils, a toxic species generated under specific pre-incubation conditions (Condello *et al*, 2015;
394 Sandberg *et al*, 2010).

395 Neuron–glia cultures were infected at day 1 in vitro (DIV1) with lentiviral constructs expressing either
396 the Flower win isoform (mFwe2), the Flower C-terminal signaling domain, or mScarlet I as a control. On
397 DIV7, cultures were treated with Alexa647-conjugated Aβ protofibrils (0.1 μM) and maintained for an
398 additional six days before analysis (Fig. 7A). Aβ exposure induced marked cytotoxicity, with ~45% of
399 neurons and ~35% of astrocytes becoming CC3-positive. Notably, overexpression of either mFwe2 or
400 the C-terminal domain significantly reduced apoptosis in both cell types, restoring survival to near
401 baseline levels comparable to untreated controls (Fig. 7B).

402 Given the central role of astrocytes in Aβ uptake and clearance(Sollvander *et al*, 2016), we asked
403 whether Flower signaling promotes a "clearance-competent" astrocyte state. Flow cytometry of
404 surviving glia revealed that while approximately 60% of WT astrocytes internalized Aβ protofibrils, this
405 proportion increased to ~75% in astrocytes expressing mFwe2, indicating enhanced uptake capacity
406 (Fig. 7C,D). Confocal imaging further demonstrated that mFwe2 expression significantly reduced the
407 size of intracellular Aβ aggregates (Fig. 7E). Consistent with this specialized phenotype, mFwe2

408 induced the expression of astrocyte activation markers *(Gfap, Lcn2*), lipid transport regulators (*Abca1,*
409 *Lrp1*), and engulfment receptors (*Megf10, Mertk*) (Fig. EV7A-E).

410 Notably, under amyloid stress, the C-terminal domain exhibited a pronounced intracellular redistribution,
411 with significant nuclear enrichment observed in both mFwe2- and C-terminal-expressing cells (Fig.
412 7A,F). To test whether this intracellular pool directly suppresses apoptotic signaling, we challenged
413 "unfit" (mFwe1-expressing) astrocytes with pro-apoptotic N-terminal peptides. Co-expression of the
414 cytosolic C-terminal domain significantly attenuated the induction of *Caspase-3* mRNA, supporting an
415 integrated neuroprotective model (Fig. 7G). In this framework, Flower "win" isoform-expressing
416 astrocytes coordinate a bifurcated response: extracellularly, they enhance Aβ uptake while potentially
417 secreting "fitness vesicles" (EVs) to eliminate distal "loser" cells; intracellularly, the C-terminal fragment
418 translocates to the nucleus to repress the apoptotic transcriptional program. This dual regulation
419 facilitates the selection of unfit cells while ensuring the survival of "win" cells around amyloid plaques,
420 thereby establishing a robust astrocytic shield against pathology (Fig. 7H).

421 Together, these results demonstrate that Flower win signaling reprograms astrocytes toward a
422 neuroprotective state, identifying the C-terminal domain as a key signaling module linking cellular fitness
423 surveillance to tissue resilience during neurodegeneration.

424

DISCUSSION

Our study uncovers a previously unrecognized mechanism by which astrocyte fitness is regulated through extracellular vesicle (EV)–mediated Flower signaling. While cellular fitness surveillance has traditionally been considered a contact-dependent process, our data demonstrate that Flower isoforms can function through non–cell-autonomous communication. Given the conserved role of fitness selection across development, aging, and disease(Coelho & Moreno, 2019; Levayer *et al*, 2016; Marques-Reis & Moreno, 2021; Merino *et al.*, 2016; Merino *et al.*, 2015; Moreno *et al*, 2015), this mechanism may represent a broader principle of tissue-level quality control that extends beyond neurodegeneration to tumor biology(Madan *et al.*, 2019; Parker *et al*, 2021).

Mechanistically, Flower integrates opposing functional signals within a single transmembrane protein. The N-terminal region promotes the elimination of less-fit cells by activating intrinsic apoptotic pathways involving *Bax* and *Caspase-3* (Chipuk & Green, 2008; Kalkavan & Green, 2018), whereas the C-terminal domain antagonizes this death signaling. This intramolecular functional polarity distinguishes Flower from multifunctional regulatory proteins such as p53, Notch, or Bcl-2 family members (Delbridge *et al*, 2016; Kannan *et al*, 2013; Maddika *et al*, 2007; Vousden & Prives, 2009; Xie *et al*, 2014), which typically rely on post-translational modification, alternative splicing, or interaction networks to mediate opposing functions.

Our topology analyses further revise previous models proposing the constitutive extracellular orientation of Flower termini (Merino *et al.*, 2013; Rhiner *et al.*, 2010). Using pH-sensitive tagging, we demonstrate that Flower domains are predominantly cytoplasmic in intact cells but become extracellularly exposed specifically upon incorporation into vesicles. This suggests that intercellular communication occurs through EV-mediated molecular presentation. Notably, the identification of Flower-positive, CD63-negative vesicles defines a specialized population we term “fitness vesicles.” Ultrastructural and colocalization analyses suggest these vesicles originate from a non-canonical biogenesis pathway distinct from classical MVB-derived exosomes. While the precise molecular machinery governing the biogenesis and unconventional secretion route of Flower remains to be fully elucidated, our data suggest a pathway that is highly sensitive to cellular fitness states and independent of traditional endosomal sorting. Similar specialization has been reported in other systems, such as lamellar body–like organelles mediating cargo delivery in keratinocytes (Rudd *et al*, 2025), suggesting an evolutionary conservation of specialized signaling vesicles for tissue quality control. These observations align with emerging views that EVs function primarily in cellular homeostasis by exporting stress-associated cargo rather than serving as high-efficiency cytoplasmic delivery vehicles (Ngo *et al*, 2025).

Isoform-specific trafficking emerged as a key determinant of competitive outcome. Despite comparable intracellular expression, the win isoform mFwe2 was secreted approximately 25-fold more efficiently than mFwe1. This suggests a secretion-based “winner-take-all” dynamic, where "win" astrocytes actively “police” the tissue by broadcasting their signaling territory. Across our experimental paradigms, the elimination of less-fit astrocytes consistently reached ~35–40%, likely reflecting intrinsic heterogeneity and a survival threshold within astrocyte networks.

463 The spatial enrichment of Flower in astrocytes surrounding Aβ plaques in both human AD brains and
464 APP-transgenic mice (Sanchez-Mico *et al.*, 2021) confirms the clinical relevance of this pathway.
465 *CACFD1* expression increased progressively with Braak stage, suggesting localized activation of
466 fitness surveillance within the neurodegenerative microenvironment. Functionally, *mFwe2* signaling
467 reprograms astrocytes toward a neuroprotective clearance state, characterized by enhanced Aβ uptake
468 and the induction of markers like *Gfap, Lcn2*, and engulfment receptors (*Megf10, Mertk*).

469 We propose that the functional coordination of Flower is governed by a "spatial paradox" resolved by
470 secretion-dependent topology and stress-induced proteolysis. Our results demonstrate that while both
471 termini are sequestered cytoplasmically in intact astrocytes, incorporation into "fitness vesicles"
472 exposes them extracellularly—a transition critical for the C-terminal domain to act as a surface-masking
473 antagonist that neutralizes N-terminal pro-apoptotic signals. Simultaneously, we find that the C-terminus
474 translocates to the nucleus under amyloid stress to repress Caspase-3 (Fig. 7). We hypothesize that
475 amyloid stress triggers a proteolytic cleavage event—potentially mediated by secretases or calpains—
476 allowing the C-terminal fragment to pivot from its role as an extracellular "surface-shield" on EVs to an
477 intracellular "nuclear-repressor" within the host cell. By coupling these spatially distinct mechanisms,
478 Flower signaling ensures that "win" astrocytes are internally "immune" to the very death signals they
479 broadcast to eliminate unfit neighbors.

480 The discovery that *CACFD1* expression is low in the healthy human brain but progressively upregulated
481 in correlation with Braak stage severity reveals a fundamental principle of human brain resilience. We
482 propose that Flower-mediated fitness surveillance serves as a "latent safeguard"—a homeostatic
483 mechanism that remains largely quiescent during health but is specifically mobilized to gate tissue
484 integrity under proteotoxic stress. By inducing a "win" phenotype in astrocytes surrounding plaques, the
485 human brain attempts to construct a biological "firewall" that isolates pathology. The transition from
486 incipient to severe Alzheimer's Disease may thus be governed by the exhaustion of this fitness-selection
487 machinery, where the astrocyte-led resilience can no longer keep pace with amyloid-induced fitness
488 loss.

489 This modularity suggests a transformative "two-sided" therapeutic platform. The N-terminal "clearance"
490 signal represents a tool for precision medicine, harnessing fitness-sensing machinery to force the
491 competitive elimination of deleterious cells, such as tumors, by the healthy stroma. Conversely, the C-
492 terminal "rescue" signal offers a blueprint for stabilizing fragile neurons. Delivering C-terminal peptides
493 could provide a critical window of "transcriptional resilience," providing reprogrammed glia the
494 necessary time to clear the toxic microenvironment and restore neuronal functional integrity. This
495 paradigm shifts the focus from merely slowing cell death to actively fostering a resilient cellular
496 environment.

497 While this study focuses on astrocyte–astrocyte interactions, Flower-dependent signaling may also
498 operate at neuron–glia interfaces. Given neurons' sensitivity to proteotoxic stress (Condello *et al.*, 2015;
499 Sandberg *et al.*, 2010), Flower-containing vesicles from astrocytes could modulate neuronal
500 vulnerability by facilitating the removal of compromised cells or delivering pro-survival cues. Although

our mechanistic conclusions rely on disease-relevant overexpression, the conserved upregulation in human AD tissue highlights Flower as a master regulator of glial resilience.

In summary, our findings establish Flower as a central regulator of astrocyte fitness and neuronal survival in Alzheimer's disease. Through isoform-specific trafficking and EV-mediated communication, Flower orchestrates competitive survival decisions that shape glial responses to neurodegenerative stress. This non-canonical signaling paradigm positions Flower as a promising therapeutic target for enhancing glial support and preserving neuronal integrity.

509 **Methods**

510 **Reagents and tools table**

Reagent/resource	Reference or source	Identifier or catalog number
Antibodies		
Pan-Flower	Generated in house. Chang et al.(Chang *et al.*, 2018)	Polyclonal, raised against full length protein and pre-absorbed against Fwe KO spleen
Flower (#1557)	Generated in house	Polyclonal, sequence-directed (targeted to C-terminal)
HA (Clone 3F10)	Roche	Cat# 11867423001, RRID:AB_390918
Flag (Clone M2)	Sigma-Aldrich	Cat# F1804, RRID:AB_262044
RFP (DsRed)	GenWay/aviva systems	Cat# OARA01891, RRID:AB_10883251
Cleaved Caspase-3	Cell signaling	Cat# 9661, RRID:AB_2341188
Iba1	FujiFilm	Cat# 019-19741, RRID:AB_839504
Iba1	Novus Biologicals	Cat# NB100-1028, RRID:AB_3148646
GFAP	Abcam	Cat# ab4674, RRID:AB_304558
GFAP	DAKO, Agilent Technologies	Cat# Z0334, RRID:AB_10013382
GFP	Abcam	Cat# ab13970, RRID:AB_300798
CD63	Abcam	Cat# ab217345, RRID:AB_2754982
GAPDH	Cell signaling	Cat #2118, RRID:AB_561053
Anti-Rabbit IgG (H+L)- Alexa Fluor488	Jackson ImmunoResearch Europe Ltd	Cat# 111-545-003, RRID AB_2338046
Anti-Rabbit IgG (H+L)- Cy3	Jackson ImmunoResearch Europe Ltd	Cat# 112-165-003, RRID:AB_2338240
Anti-mouse IgG (H+L)- Alexa Fluor488	Invitrogen	Cat# A-11001, RRID:AB_2534069
Anti-mouse IgG (H+L)- Alexa Fluor647	Invitrogen	Cat# A-21235, RRID:AB_2535804
Anti-chicken IgY (H+L)- Alexa Fluor488	Invitrogen	Cat# A-11039, RRID:AB_2534096
Anti-chicken IgY (H+L)- Alexa Fluor568	Invitrogen	Cat# A-11041, RRID:AB_2534098
Anti-rabbit IgG (H+L)- Alexa Fluor568	Invitrogen	Cat# A-11011, RRID:AB_143157
Anti-rabbit IgG (H+L)- Alexa Fluor647	Invitrogen	Cat# A-21244, RRID:AB_2535812
Anti-rat IgG (H+L)- Alexa Fluor488	Invitrogen	Cat# A-11006, RRID:AB_2534074
Anti-rat IgG (H+L)- Alexa Fluor568	Invitrogen	Cat# A-11077, RRID:AB_2534121
Anti-goat IgG (H+L)- Alexa Fluor647	Invitrogen	Cat# A-21447, RRID:AB_2535864

Anti-mouse IgG (H+L)-HRP	Invitrogen	Cat# 32430, RRID:AB_1185566
Anti-rabbit IgG (H+L)- HRP	EMD Millipore	Cat# AP307P, RRID:AB_92641
Anti-Rat IgG (H+L)-HRP	GE healthcare	Cat# NA935, RRID:AB_772207
Anti-rabbit IgG (H+L) 10 nm gold labeled	Aurion	Cat# 810.011 polyclonal
Anti-mouse IgG (H+L) 6 nm gold labeled	Aurion	Cat# 806.022 polyclonal
Anti-Rat IgG (H+L) 10 nm gold labeled	Aurion	Cat# 810.055 polyclonal
Anti-rabbit IgG (H+L) 6 nm gold labeled	Aurion	Cat# 806.011 polyclonal
Anti-mouse IgG (H+L) 15 nm gold labeled	Aurion	Cat# 815.022 polyclonal
Bacterial and virus strains		
One Shot™ TOP10 Chemically Competent *E. coli*	Invitrogen	Cat# C404003
One Shot™ Stbl3™ Chemically Competent *E. coli*	Invitrogen	Cat# C737303
NEB® Stable Competent *E. coli* (High Efficiency)	New England Biolabs	Cat# C3040H
Lentivirus: pCDH-mFwe2-mScarlet-I	This study	N/A
Lentivirus: pCDH-mFwe-C-terminal-mScarlet-I	This study	N/A
Packaging plasmid: pMDLg/pRRE	Addgene	Cat# 12251
Packaging plasmid: pRSV-Rev	Addgene	Cat# 12253
Envelope plasmid: pMD2.G (VSV-G)	Addgene	Cat# 12259
Chemicals, peptides, and recombinant proteins		
TRIzol Reagent	Invitrogen	Cat# 15596026
Chloroform	Sigma-Aldrich	Cat# 288306
Congo Red	Sigma-Aldrich	Cat# C6277
DAPI (4',6-diamidino-2-phenylindole)	Thermo Fisher Scientific	Cat# 10116287
Thioflavin-S (Thio-S)	Sigma-Aldrich	Cat# T1892
Carbonyl cyanide 3-chlorophenylhydrazone (CCCP)	Sigma-Aldrich	Cat# C2759
#1824 Fwe Exon3 (Sequence: FCCQFVEFANTVAEKVDRLRRSWQKAVFYC)	This study	N/A
#1825 Fwe N ter. (Sequence: MSGSGAAGAAAGPAPPAQEEGMTWWYRWLCR)	This study	N/A
#1826 Fwe C ter. (Sequence: GKKGDAISYARIQQQRQQADEEKLAETFEGEL)	This study	N/A
#1562II Fwe C ter. (Cys in N term) (Sequence: c-GKKGDAISYARIQQQRQQADEEKLAETFEGEL)	This study	N/A
Fwe Exon3 (long) (Sequence: Biotin-MNAFILLLCEAPFCCQFVEFANTVAEKVDRLRRSWQKAVFYC)	Biozol/biomatik	N/A
Beta-Amyloid$_{1-42}$, HiLyte™ Fluor 647-labeled (sequence: HiLyte Fluor™ 647-DAEFRHDSGYEVHHQKLVFFAEDVGSNKGAIIGLMVGGVVIA)	AnaSpec	Cat# AS-60479-01

Critical commercial assays		
ABScript II cDNA Synthesis Kit	ABclonal	Cat# RK20400
Phusion High-Fidelity PCR Master Mix	Thermo Fisher Scientific	Cat# F530S
RNeasy FFPE kit	Qiagen	Cat# 73504
Genious 2xSYBR Green Fast qPCR Mix	ABclonal	Cat# RK21205
QIAquick Gel Extraction Kit	Qiagen	Cat# 28706
Plasmid Mini Kit	Qiagen	Cat# 27106
EndoFree Plasmid Maxi Kit	Qiagen	Cat# 12362
Nucleofection kit for primary glia cells	Lonza	Cat# VPI-1006
CellTrace™ CFSE Cell Proliferation Kit	Thermo Fisher Scientific	Cat# C34554
Deposited data		
Raw images and gel	This study	Separated file
Experimental models: Cell lines		
Lenti-X 293T cell line	Takara Bio / Clontech	Cat# 632180
Experimental models: Organisms/strains		
C57BL/6N wild type mice	This study	N/A
Fwe KO transgenic mice	This study	PMID: 29288152
APP/PS1 transgenic mice (APPtg)	Gift from Prof. Mathias Jucker, Hertie Institute for Clinical Brain Research, Tübingen, Germany(Radde *et al*, 2006)	N/A
Oligonucleotides		
mFwe1 qPCR Forward: ACTGACTCATCCAATAACAGG	This paper	N/A
mFwe1 qPCR Reverse: ACCATGCCTACACATACATTAG	This paper	N/A
mFwe2 qPCR Forward: GCCATTTCTTATGCTCGGAT	This paper	N/A
mFwe2 qPCR Reverse: GCCATTTAACAGAGCTGACA	This paper	N/A
mFwe3 qPCR Forward: GTCTTCTACTGCGGGCAT	This paper	N/A
mFwe3 qPCR Reverse: AGAGGGAAATGGTGTTTCTG	This paper	N/A
mFwe4 qPCR Forward: TTGCTAAATCCTGGGTGTCC	This paper	N/A
mFwe4 qPCR Reverse: TGTTCAGAGGGTGGATAGTG	This paper	N/A
Bax qPCR Forward: CTACAGGGTTTCATCCAG	This paper	N/A
Bax qPCR Reverse: TATTGCTGTCCAGTTCATCT	This paper	N/A
Bcl2 qPCR Forward: TACCTGAACCGGCATCT	This paper	N/A
Bcl2 qPCR Reverse: CAGCCAGGAGAAATCAAACA	This paper	N/A
Casp3 qPCR Forward: GGCTTGCCAGAAGATAC	This paper	N/A
Casp3 qPCR Reverse: CTCCAGGAATAGTAACCAG	This paper	N/A
Gfap qPCR Forward: AAATTGCTGGAGGGCGAAGAA	This paper	N/A
Gfap qPCR Reverse: TGTGAGCCTTTTGAGAGGTCTT	This paper	N/A

Lcn2 qPCR Forward: AATGTCACCTCCATCCTGGTC	This paper	N/A
Lcn2 qPCR Reverse: GCCACTTGCACATTGTAGCTC	This paper	N/A
C3 qPCR Forward: TCCCAGCTACTAGTGCTACTG	This paper	N/A
C3 qPCR Reverse: CAGTACGATGGTCTCTTCGC	This paper	N/A
Serping1 qPCR Forward: AGTGCCCATGATGAGTAGCG	This paper	N/A
Serping1 qPCR Reverse: CACGGGTACCACGATCACAA	This paper	N/A
S100a10 qPCR Forward: GACAAAGGAGGACCTGAGAGTG	This paper	N/A
S100a10 qPCR Reverse: CTCTGGAAGCCCACTTTGCCAT	This paper	N/A
Ptx3 qPCR Forward: CAATGGACTTCATCCCACCGA	This paper	N/A
Ptx3 qPCR Reverse: ACAGCTTGTCCCACTCCGA	This paper	N/A
Megf10 qPCR Forward: CAGCGCCTATGATGGGGAAT	This paper	N/A
Megf10 qPCR Reverse: CACTGCCCCGAGATATGGTC	This paper	N/A
Mertk qPCR Forward: CGCTCAGACAATGGGTCGT	This paper	N/A
Mertk qPCR Reverse: AAGGCTGTGTTTCTGGTGACA	This paper	N/A
Lrp1 qPCR Forward: GTATTGAGCGGTCTCGCCTT	This paper	N/A
Lrp1 qPCR Reverse: CATCCGAGCATCACACCAGT	This paper	N/A
Abca1 qPCR Forward: TAGCAGCACCGTGTCTTGTC	This paper	N/A
Abca1 qPCR Reverse: GCGTGTCACTTTCATGGTCG	This paper	N/A
GAPDH qPCR Forward: GTATGTCGTGGAGTCTACTG	This paper	N/A
GAPDH qPCR Reverse: TATTTCTCGTGGTTCACACC	This paper	N/A
Recombinant DNA		
pMax-mFwe1-mTFP	Ravichandran et al.(Ravichandran *et al.*, 2024)	PMID: 39694922
pMax-mFwe2-mTFP	Ravichandran et al.(Ravichandran *et al.*, 2024)	PMID: 39694922
pMax-mFwe3-mTFP	Ravichandran et al.(Ravichandran *et al.*, 2024)	PMID: 39694922
pMax-mFwe4-mTFP	Ravichandran et al.(Ravichandran *et al.*, 2024)	PMID: 39694922
pMax-mFwe1-Cherry	This study	N/A
pMax-mRFP-mFwe2	This study	N/A
pMax-mFwe3-Cherry	This study	N/A
pMax-mFwe4-Cherry	This study	N/A

pMax-hFwe3-mTFP	Ravichandran et al.(Ravichandran *et al.*, 2024)	PMID: 39694922
pMax-hFwe4-mTFP	Ravichandran et al.(Ravichandran *et al.*, 2024)	PMID: 39694922
pMax-hFwe3-mCherry	This study	N/A
pMax-hFwe4-mCherry	This study	N/A
pMax-HA-mFwe N ter.-mScarlet I-TM	This study	N/A
pMax-HA-mFwe Exon3-mScarlet I-TM	This study	N/A
pMax-HA-mFwe C ter.-mScarlet I-TM	This study	N/A
pMax-pHluorin2	This study	N/A
pMax-Syb2-pHluorin2	Chang et al.(Chang *et al.*, 2018)	PMID: 29288152
pMax-mFwe1-pHluorin2	This study	N/A
pMax-mFwe2-pHluorin2	This study	N/A
pMax-pHluorin2-mFwe1	This study	N/A
pMax-pHluorin2-mFwe2	This study	N/A
pMax-3xFlag-mFwe1-3xHA	This study	N/A
pMax-3xFlag-mFwe2-3xHA	This study	N/A
pMax-3xFlag-mFwe3-3xHA	This study	N/A
pMax-3xFlag-mFwe4-3xHA	This study	N/A
pMAX-CD63lys-pHuji-CD63	Alawar et al.(Alawar *et al*, 2026)	?
pCDH-mFwe2-mScarlet-I	This study	N/A
pCDH-mFwe-C-terminal-mScarlet-I	This study	N/A
pMDLg/pRRE	Addgene	Cat# 12251
pRSV-Rev	Addgene	Cat# 12253
pMD2.G (VSV-G)	Addgene	Cat# 12259
Software and algorithms		
Fuji	Schindelin et al.(Schindelin *et al*, 2012)	RRID: SCR_002285
SigmaPlot, version 14.5	Systat Software Inc.	https://systatsoftware.com/sigmaplot
FlowJo	Becton, Dickinson and Company (BD)	https://www.flowjo.com
Bio-Rad Manager	Bio-Rad Laboratories	https://www.bio-rad.com/en-us/product/cfx-manager-software
BioRender	BioRender.com	https://biorender.com
CorelDRAW Graphics Suite	Corel Corporation	https://www.coreldraw.com

511

512 **Mice**

513 Fwe KO mice were generated as previously described(Chang *et al.*, 2018). APP/PS1 transgenic mice
514 (APP^{tg}), which overexpress human mutated APP (KM670/671NL) and PS1 (L166P) under the control
515 of Thy1 promoters (PMC1559665), were kindly provided by M. Jucker (Hertie Institute for Clinical Brain
516 Research, Tübingen, Germany). The KO, transgenic and WT mice used in this study were on a
517 C57BL/6N background. Fwe KO pups used for astrocyte isolation were postnatal day 0–2 (P0–P2).
518 Adult WT and APP mice used for brain tissue staining and RNA analysis were 60-70 weeks old and

519 included both sexes. Animals were housed at 22 °C with 50–60% humidity under a 12 h light/dark cycle.
520 All experimental procedures were approved by the local regulatory authority of Saarland (Landesamt
521 für Verbraucherschutz; protocols AZ: 2.4.1.1/11-2021 to E.K. and VM2023-05 to Y.L.) and carried out in
522 accordance with institutional and governmental guidelines.

523

524 **Human postmortem brain tissue**

525 Formalin-fixed, paraffin-embedded hippocampal sections from autopsy-confirmed Alzheimer's disease
526 (AD) patients were obtained from the Department of Neuropathology, Saarland University, Germany.
527 The use of human tissue was approved by the Ärztekammer des Saarlandes (Ethics Committee of the
528 Medical Association of Saarland), approval number 106/25. These paraffin-embedded hippocampal
529 sections were used for immunostaining experiments as described in the Method Details section.

530

531 **Primary cortical neuron and astrocyte culture**

532 Cortical neurons and astrocytes were isolated from P0–P2 mouse pups. Cerebral hemispheres were
533 dissected in ice-cold Earle's Balanced Salt Solution (EBSS; Gibco). Following removal of the meninges,
534 cortices were minced into small fragments and enzymatically digested with 35 U/mL papain
535 (Worthington) at 37 °C for 45 min, followed by gentle mechanical trituration to obtain a single-cell
536 suspension. For neuronal culture, dissociated cells were seeded onto 25 mm glass coverslips placed
537 in 6-well culture plates at a density of 3×10^5 cells per coverslip. Coverslips were pre-coated with a
538 solution containing 17 mM acetic acid, collagen I (Gibco), and poly-D-lysine (Sigma). On day in DIV 1,
539 the culture medium was replaced to remove residual debris. Neurons were maintained in Neurobasal-
540 A (NBA) medium supplemented with 10% FCS, 1% penicillin-streptomycin (Invitrogen), 1% GlutaMAX,
541 and 2% B27 supplement (Gibco). Neurons were cultured for 9–12 days prior to experimental use. For
542 astrocyte culture, dissociated cortical cells were seeded into T-75 culture flasks (one brain per flask),
543 pre-coated with poly-L-ornithine (Sigma). On DIV1, flasks were rinsed and vigorously agitated with
544 DPBS to remove debris and non-adherent cells. The remaining adherent astrocytes were cultured in
545 Dulbecco's Modified Eagle Medium (DMEM; Gibco) supplemented with 10% FCS and 1% penicillin-
546 streptomycin for 9–14 days before use in experiments.

547

548 **Flower antibody generation**

549 Details of Flower antibody generation have been previously described(Chang *et al.*, 2018). In this study,
550 two custom-made polyclonal antibodies were used. The first, referred to as Flower antibody #1557, was
551 sequence-directed and raised against the C-terminal 18 amino acids shared by mFwe2 and mFwe4.
552 The second, a pan-Flower antibody, was generated against the untagged full-length recombinant
553 mFwe2 protein(Chang *et al.*, 2018) and recognizes multiple epitopes across the Flower protein,
554 including both N- and C-terminal regions.

555

556 **Peptides synthesis**

557 Peptides were synthesized with an automated ResPepSL synthesiser (Intavis) using amide Rink resin
558 as the solid phase and Fmoc-protected amino acids (Carbolution) for coupling according to the method
559 of Merrifield(Merrifield, 1963). The resin-coupled peptides were cleaved and deprotected with
560 trifluoroacetic acid (Sigma Aldrich) followed by precipitation with tert-butyl methyl ether (Fisher Scientific)
561 and further analysis and purification by preparative HPLC (Merck) (purtity > 90%). Lyophilized peptides
562 (Lyovac GT2, Finn-Aqua) were stored at 4 °C. Stock solutions of the peptides were prepared fresh and
563 used the same day.

564

565 **Mouse brain slice preparation and staining**

566 APP-transgenic mice and age-matched WT littermates were sacrificed by CO_2 inhalation followed by
567 decapitation. Brains were extracted and post-fixed in 4% paraformaldehyde (PFA) at 4 °C for 24 h. Fixed
568 tissues were sectioned into 30 µm slices using a vibratome (Leica VT1000 S). Sections were washed
569 three times with Dulbecco's PBS (D-PBS), permeabilized with 0.1% Triton X-100 for 10 min, and
570 blocked with 10% fetal calf serum (FCS) for 30 min at room temperature (RT). Primary antibodies rabbit
571 anti-Iba1 (1:200, 019-19741; FujiFilm), goat anti-Iba1 (1:200, NB100-1028; Novus Biologicals), chicken
572 anti-GFAP (1:1000, ab4674; Abcam) and polyclonal rabbit anti-Flower #1557 (1:200, homemade) were
573 applied overnight at 4 °C, followed by incubation with corresponding Alexa Fluor-conjugated secondary
574 antibodies (Invitrogen, 1:1000). Nuclei were counterstained with DAPI, and slices were mounted and
575 imaged by confocal microscopy.

576

577 **Immunostaining of postmortem human brain sections from AD patients**

578 Formalin-fixed, paraffin-embedded hippocampal sections from autopsy-confirmed Alzheimer's disease
579 (AD) patients were obtained from the Department of Neuropathology, Saarland University, Germany.
580 The use of human tissue was approved by the Ärztekammer des Saarlandes (Ethics Committee of the
581 Medical Association of Saarland), approval number 106/25. Following deparaffinization, slides were
582 subjected to antigen retrieval in citrate buffer (pH 6.0) for 30 min. Endogenous peroxidase activity was
583 quenched with 3% H_2O_2 in PBS, and sections were blocked for 1 h in 0.2% casein.

584 Immunostaining was performed using a rabbit polyclonal anti-GFAP antibody (1:500, Z0334; DAKO,
585 Agilent Technologies, Waldbronn, Germany), followed by detection with an alkaline phosphatase (AP)-
586 conjugated goat anti-rabbit IgG secondary antibody (DAKO) and visualization using the Vector Red
587 Substrate Kit (SK-5100; Vector Laboratories, Newark, USA).

588 To assess astrocytic localization of Flower protein, serial sections were stained with a rabbit polyclonal
589 anti-Flower antibody, followed by GFAP staining. Detection was performed with either AP- or
590 horseradish peroxidase (HRP)-conjugated goat anti-rabbit IgG secondary antibodies (both from DAKO),
591 and developed with either 3,3'-diaminobenzidine tetrahydrochloride (DAB; Sigma) or the Vector® Blue
592 Substrate Kit (SK-5300; Vector Laboratories). Slides were counterstained with hematoxylin.

593 For fluorescence-based colocalization analysis, the same staining protocol was repeated using Alexa
594 Fluor 488- or Cy3-conjugated goat anti-rabbit IgG secondary antibodies (Jackson ImmunoResearch
595 Europe Ltd, Cambridgeshire, UK). Colocalization between Flower and GFAP was evaluated by confocal
596 microscopy (LSM 780, Zeiss).

597

598 **Human Alzheimer's disease transcriptome analysis**

599 Transcriptome data from hippocampal specimens derived from patients with Alzheimer's disease (AD)
600 of varying disease severity, as well as from non-demented control individuals, were obtained from the
601 Gene Expression Omnibus (GEO) database (Blalock *et al.*, 2004) (accession number GSE1297).
602 Expression values of CACFD1 were extracted from the dataset and normalized to z-scores by
603 subtracting the dataset mean and dividing by the standard deviation. Differences in CACFD1 expression
604 among groups were assessed using a two-tailed Kruskal–Wallis test. Statistical analyses were
605 performed using GraphPad Prism version 10.2.3. The analysis protocol was approved by the
606 Institutional Research Ethics Committee of China Medical University Hospital, Taiwan (CMUH113-
607 REC1-167).

608

609 **Cell fitness assay**

610 To assess the fitness effects of Flower isoforms, Flower KO astrocytes cultured for 9–12 days were
611 used. Cells were detached using Trypsin-EDTA, washed three times with DPBS, and resuspended in
612 100 μL nucleofection solution (Basic Nucleofector Kit for Primary Mammalian Glial Cells, Lonza). Each
613 nucleofection was performed with 4×10^6 astrocytes and 5 μg plasmid DNA encoding fluorescently
614 tagged win or lose Flower isoforms. Electroporation was carried out using a electroporation device
615 (Lonza NucleofectorI/II/2b System). Following electroporation, equal numbers of the two transfected
616 astrocyte populations were mixed and co-seeded into 6-well plates containing 25 mm coverslips
617 (around 4×10^5 mixed cells per coverslip) in the following combinations: win+win, win+lose, and
618 lose+lose. To evaluate the role of specific Flower protein domains in cell competition, three additional
619 constructs were generated, each encoding a truncated version of Flower fused to mScarlet I-TM,
620 targeting either the N-terminus, Exon 3, or C-terminus. These constructs were individually transfected
621 into Flower KO astrocytes and co-cultured with an equal number of Flower KO astrocytes expressing
622 the lose isoform. After 24 h of co-culture, cells were fixed in 4% PFA for 10 min at RT. DAPI was added
623 prior to fixation to label late apoptotic cells. Immunocytochemistry was performed using a rabbit anti-
624 Cleaved Caspase-3 antibody (1:500, #9661; Cell Signaling) to detect early apoptotic cells.

625 For peptide-based assays, synthetic peptides corresponding to the N-terminus, Exon 3, and C-terminus
626 regions of Flower were added to astrocyte cultures at a concentration of 1 μg/ml. Astrocytes expressing
627 either win or lose isoforms were treated for 24 h prior to fixation and analysis. Finally, Live or fixed cells
628 were imaged using a confocal microscope (LSM780, Zeiss) equipped with a 40×/1.3 NA objective. Cell
629 counts and cell death analysis were performed manually using Fiji (ImageJ).

630 To evaluate the role of secreted Flower in cell fitness, supernatants from T-75 flasks were collected,
631 and EVs were isolated by ultracentrifugation (see EV isolation). Approximately 20 µg of protein from the
632 pelleted supernatant can be obtained from one flask (10 ml). Ten micrograms of pelleted EVs were
633 applied to approximately 1×10^5 unfit astrocytes expressing mFwe1-mCherry, which were seeded on a
634 12.5 mm coverslip for the fitness assay. After 24 h, cells were fixed and stained for CC3 to quantify
635 apoptotic cells.

636

637 **Amyloid Beta1–42 protofibril generation and application**

638 Synthetic $A\beta_{1-42}$ peptides labeled with HiLyte Fluor 647 (Anaspec Inc.) were dissolved in 1% NH_4OH
639 and subsequently diluted in 1x PBS to a final concentration of 100 µM. The solution was incubated at
640 37 °C for 4 h to allow for protofibril formation. Protofibrils were then diluted to a final concentration of
641 0.1 µM and applied to cortical neuron cultures on DIV 7 for 6 days to assess cytotoxicity. WT cortical
642 neuron cultures were transduced with lentiviruses encoding mFwe2-mScarlet I, mFwe C-terminal-
643 mScarlet I, or cytosolic mScarlet I at DIV 1. Cells were then either fixed and immunostained for
644 apoptosis analysis, collected for flow cytometry to assess $A\beta_{1-42}$ protofibril uptake, or harvested for RNA
645 extraction followed by qPCR analysis.

646

647 **Plasmid cloning**

648 Plasmids encoding mouse Fwe1, Fwe2, Fwe3, and Fwe4, as well as human Fwe3 and Fwe4 with C-
649 terminal mTFP tags, were generated in a previous study(Ravichandran *et al.*, 2024). These constructs
650 served as the backbone for the generation of additional tagged and truncated Flower expression
651 plasmids used in this study.

652 To generate C-terminal mCherry fusion constructs (pMax-mFwe1-Cherry, pMax-mFwe3-Cherry, pMax-
653 mFwe4-Cherry, pMax-hFwe3-mCherry, and pMax-hFwe4-mCherry), the mTFP sequence in the
654 parental pMax-mFwe-mTFP plasmids was replaced with mCherry using XbaI and XhoI restriction sites.
655 For pMax-mRFP-mFwe2, the mRFP sequence was cloned upstream of the mFwe2 coding sequence.

656 For generation of truncated Flower constructs fused to a transmembrane (TM) domain, the pDisplay-
657 pHuji vector (#61556, Addgene), containing the PDGFR TM domain, was used as a template. The
658 mScarlet-I sequence and PDGFR TM domain were subcloned into the pMax backbone to generate a
659 pMax-mScarlet-I-TM vector. Truncated Flower sequences corresponding to the N-terminal region, exon
660 3, or C-terminal region were PCR-amplified using gene-specific primers. The C-terminal Flower
661 fragment flanked by BglII and BamHI sites was synthesized (BioCAT) in pBluescript II SK(+). These
662 fragments were subcloned into pMax-mScarlet-I-TM to generate pMax-HA-mFwe-N-ter-mScarlet-I-TM,
663 pMax-HA-mFwe-Exon3-mScarlet-I-TM, and pMax-HA-mFwe-C-ter-mScarlet-I-TM constructs.

664 To generate dual-tagged Flower constructs, synthetic DNA fragments encoding either a 3×Flag tag
665 (flanked by ClaI and EcoRI sites) or a 3×HA tag (flanked by XbaI and XhoI sites) were obtained from
666 BioCAT. The 3×Flag sequence replaced mScarlet-I, and the 3×HA sequence replaced mTFP in the

667 corresponding pMax-mFwe plasmids, resulting in pMax-3×Flag-mFwe1-3×HA, pMax-3×Flag-mFwe2-
668 3×HA, pMax-3×Flag-mFwe3-3×HA, and pMax-3×Flag-mFwe4-3×HA.

669 The pmax-CD63-pHuji was generated by subcloning from pCMV-CD63-pHuji into pMax with the
670 restriction sites EcoRI and XbaI. Its size was 4.282 kb. pCMV-CD63-pHuji was a generous gift from
671 Frederik Verweij (Centre de Psychiatrie et neurosciences, Amsterdam/Paris). In the construct the pH
672 sensitive fluorescent marker protein was located to the first extracellular loop of the tetraspanins facing
673 the acidic lumen of the organelles(Verweij *et al.*, 2018).

674 For pHluorin2-based constructs, pHluorin2 was PCR-amplified and cloned either C-terminally or N-
675 terminally. For C-terminal fusions (pMax-mFwe1-pHluorin2 and pMax-mFwe2-pHluorin2), the mTFP
676 sequence was replaced by pHluorin2 using XbaI and XhoI. For N-terminal fusions (pMax-pHluorin2-
677 mFwe1 and pMax-pHluorin2-mFwe2), the Halo tag in pMax-Halo-mFwe constructs was replaced with
678 pHluorin2 using EcoRI and NheI. pMax-Syb2-pHluorin2 was generated previously[4].

679 For lentiviral expression, the pCDH-EF1 vector (#72266, Addgene) was used. mFwe2 was cloned into
680 pCDH-EF1 using EcoRI and XbaI, followed by insertion of mScarlet-I to generate pCDH-mFwe2-
681 mScarlet-I. To generate pCDH-mFwe-C-terminal-mScarlet-I, the C-terminal Flower fragment was PCR-
682 amplified and used to replace the full-length mFwe2 sequence in the pCDH-mFwe2-mScarlet-I
683 backbone. All constructs were verified by Sanger sequencing using gene-specific primers (Microsynth
684 Seqlab).

685

686 **Surface plasmon resonance binding analysis**

687 Series Sensor Chips CM5 were obtained from Cytiva (Freiburg, Germany). Amine coupling reagents N-
688 (3-dimethylaminopropyl)-N'-ethylcarbodiimide hydrochloride (EDC) and N-hydroxysuccinimide (NHS),
689 along with ethanolamine hydrochloride, were purchased from Merck KGaA (Darmstadt, Germany).
690 HEPES buffer, NaCl, and NaOH were sourced from Carl Roth (Karlsruhe, Germany), Grüssing GmbH
691 (Filsum, Germany), and VWR Chemicals (Darmstadt, Germany), respectively. TWEEN 20 and dimethyl
692 sulfoxide (DMSO) were acquired from Sigma-Aldrich (Steinheim, Germany) and Thermo Fisher
693 Scientific (Dreieich, Germany). For SPR analysis, HBS-P (0.01 M HEPES, 0.15 M NaCl, 0.05% TWEEN
694 20) served as running buffer during surface preparation. All glassware was rinsed with 50 mM NaOH
695 and Milli-Q water before use. Ligand 1562II was immobilized onto a CM5 sensor chip via amine coupling
696 using a BIACORE T200 system (Cytiva, Freiburg, Germany). Carboxyl groups were activated with a
697 1:1 mixture of 391.2 mM EDC and 100 mM NHS (10 µl/min, 7 min). 1562II (200 µg/ml in 10 mM HEPES,
698 pH 5.5) was injected for 2 min (10 µl/min), achieving an immobilization level of about 4690 RU. Residual
699 esters were blocked with 1 M ethanolamine-HCl (pH 8.5, 7 min). A reference surface was prepared by
700 activation and immediate deactivation without ligand.
701 Binding of 1825 and 1826 to immobilized 1562II was assessed at 25 °C using HBS-P with 3 % DMSO
702 as running buffer. Solvent correction was performed using DMSO dilutions (2.5 - 3.8 %). Analytes were
703 prepared at 15, 30, and 40 µM in running buffer and injected in triplicate. Each cycle included a 180 s
704 association and 300 s dissociation phase at 30 µl/min. Surfaces were washed with running buffer and
705 cleaned with 50 % DMSO. Regeneration was achieved using 5 M NaCl followed by deionized water.

706 Data were processed with BIACORE T200 Evaluation Software v3.2.1, applying double referencing and
707 solvent correction prior to curve fitting.
708

709 **Harvest of secreted Flower fractions and extracellular vesicles**

710 WT astrocytes cultured for 9–12 days were electroporated with constructs expressing mFwe2-pHluorin2,
711 3×Flag-mFwe1-3×HA, or 3×Flag-mFwe2-3×HA. Following electroporation, 4 × 10^6 cells were cultured
712 in a T-75 flask containing 10 ml of culture medium for 2–3 days. The medium was supplemented with
713 10% exosome-depleted FCS, prepared by ultracentrifuging heat-inactivated FCS (Gibco) at 100,000 ×
714 g for 16 h at 4 °C to remove serum-derived EVs. To harvest astrocyte-derived EVs, conditioned medium
715 was collected and centrifuged at 300 × g for 10 minutes to remove cells and large debris, followed by
716 an additional centrifugation step at 2,000 × g for 20 min to further eliminate residual cell debris and
717 dead cells. The supernatant was then filtered through a 0.22 µm syringe filter (Millipore) to eliminate
718 residual debris and large vesicles. Sequential ultracentrifugation was performed: first at 10,000 × g for
719 40 minutes at 4 °C to remove apoptotic bodies, followed by 100,000 × g for 1 h and 15 minutes at 4 °C
720 to pellet secreted Flower-containing fractions and EVs. The resulting pellet was resuspended in D-PBS
721 and washed by a second ultracentrifugation step at 100,000 × g for 1 h and 15 min at 4 °C to reduce
722 contaminating soluble proteins. All ultracentrifugation steps were carried out using Ultra-Clear
723 centrifuge tubes (Beckman Coulter) in an Optima XPN-80 ultracentrifuge (Beckman Coulter). For
724 analysis of secreted Flower and EV content, pellets were resuspended in D-PBS and applied to
725 12.5 mm coverslips pre-coated with poly-L-ornithine. After a 1 h incubation at RT, the supernatant was
726 carefully removed to avoid disturbing the settled EVs. The samples were then fixed with 4% PFA for 20
727 min, followed by immunostaining.

728

729 **EV particle size analysis**

730 EVs harvested from GFP, mFwe1 or mFwe2-overexpressing WT astrocyte cultures were analyzed by
731 asymmetric-flow field-flow fractionation (AF4) using an Eclipse system (Wyatt Technology, Santa
732 Barbara, CA, USA) coupled to an Agilent 1260 Infinity II LC (Agilent Technologies, Waldbronn,
733 Germany). Online detection included multi-angle light scattering (MALS; DAWN, 18 angles, 658 nm,
734 Wyatt Technology), differential refractive index (dRI; Optilab, Wyatt Technology), and UV–Vis (Agilent
735 1260 DAD) measurements. Instrument control and sequence execution were performed using VISION
736 v2.x (Wyatt Technology), and data were processed in ASTRA v7.3 (Wyatt Technology). Following a
737 focus step, samples were eluted under programmed cross-flow at a constant detector flow. Geometric
738 radii were calculated slice-wise in ASTRA using a spherical Lorenz–Mie model, specifying the material
739 refractive index, and entering the refractive index increment (dn/dc) or extinction coefficients as
740 appropriate for dRI or UV–Vis detection. Absolute particle number concentrations were obtained using
741 ASTRA's "Number from Light Scattering" analysis, with number density per slice integrated over each
742 elution peak and normalized to the injected volume. Prior to sample analysis, detectors were aligned
743 and normalized according to manufacturer procedures, membranes were conditioned, and a
744 monodisperse polystyrene latex standard was used to verify retention behavior and MALS response.

745 Mobile-phase blanks were injected between samples to monitor carryover and baseline stability(Cho &
746 Hackley, 2010).

747

748 **Immunogold labeling and electron microscopy**

749 After size analysis and quantification, 40 µl of each EV sample were fixed with PFA (2% final
750 concentration). For immunogold analysis, 7 µl of the fixed EVs were dropped onto pioloform-coated
751 200-mesh copper grids for 45 min. After several washing steps with D-PBS and 50 mM glycine in D-
752 PBS for 10 min, the grids were incubated in blocking solution (Aurion) for another 10 min. The primary
753 antibodies anti-HA (1:10), anti-Flag (1:10), anti-RFP (1:50) and the pre-absorbed anti-Flower (1:2) were
754 diluted in incubation solution (D-PBS supplemented with 0.1 % BSAc (Aurion), pH 7.4), and the grids
755 were incubated for 2 hours at 20 ±2 °C. After several washes the grids were incubated for 1 hour at 20
756 ±2 °C with the secondary gold-conjugated antibodies goat anti-rabbit (6 nm or 10 nm), goat-anti rat (10
757 nm), goat anti-mouse (6 nm or 15 nm) (Aurion), diluted in incubation solution (1:30). The samples were
758 then washed in several drops of D-PBS, fixed in 1% glutaraldehyde, rinsed with six drops of destilled
759 water, and contrasted with uranyl acetate. The grids were analyzed with a Tecnai G2 Biotwin electron
760 microscope (Thermo Fisher Scientific) and electron micrographs were acquired using Olympus iTEM
761 5.0 image software (build1243).

762

763 **Western blot analysis**

764 Cells were lysed on ice using a buffer containing 50 mM Tris-HCl (pH 7.4), 1 mM EDTA, 250 µM PMSF,
765 1% Triton X-100, 150 mM NaCl, 1 mM DTT, 1 mM sodium deoxycholate, and a protease inhibitor
766 cocktail (Roche). Cell lysis was facilitated by mechanical scraping, followed by incubation on ice for 30
767 min. Lysates were centrifuged at 16,000 × g for 10 min at 4 °C, and the supernatants were collected for
768 subsequent analysis. Protein concentrations were determined using the Pierce 660 nm Protein Assay
769 (Thermo Fisher Scientific) according to the manufacturer's instructions.

770 Equal amounts of protein (30 µg per lane for cell lysates, 10 µg per lane for secreted Flower fractions
771 from conditional medium) were resolved by SDS–PAGE using NuPAGE precast gels (Invitrogen) and
772 transferred onto nitrocellulose membranes. Membranes were blocked for 30 min at RT in TBS-T buffer
773 (20 mM Tris-HCl, 150 mM NaCl, 0.05% Tween-20, pH 7.4) containing 5% (w/v) non-fat dry milk.
774 Membranes were then incubated with primary antibodies rabbit polyclonal anti-Pan Flower (1:1000,
775 homemade), rat anti-HA (1:1000, clone 3F10, Roche), mouse anti-Flag (1:1000, clone M2, Sigma-
776 Aldrich), rabbit anti-GAPDH (1:5000, clone 14C10, Cell Signaling) and rabbit anti-CD63 (1:500, clone
777 EPR21151, Abcam) overnight at 4 °C. After washing three times in TBS-T, membranes were incubated
778 with HRP-conjugated secondary antibodies for 45 min at RT. Signal detection was performed using
779 enhanced chemiluminescence reagents (SuperSignal West Dura Chemiluminescent Substrate,
780 Thermo Fisher Scientific), and images were acquired using the FluorChem E documentation system
781 (BioLabTec GbR).

782

783 **Immunofluorescence**

784 Cells grown on coverslips were fixed in 4% PFA for 10 min at RT and subsequently washed three times
785 with D-PBS. Permeabilization was performed in D-PBS containing 0.1% Triton X-100 (Roth) for 10 min.
786 Samples were then incubated in blocking buffer (D-PBS supplemented with 2% BSA) for 30 min to
787 reduce non-specific binding. Primary antibodies rabbit polyclonal anti-Pan Flower (1:100, homemade),
788 rat anti-HA (1:100, clone 3F10, Roche), and mouse anti-Flag (1:100, clone M2, Sigma-Aldrich), rabbit
789 anti-RFP (DsRed) (1:200, OARA01891, GenWay/aviva systems) were diluted in blocking buffer and
790 applied for 1 h at RT. Following three washes with D-PBS, samples were incubated with the appropriate
791 Alexa Fluor-conjugated secondary antibodies (1:1000, Invitrogen) for 45 min at RT in the dark. After
792 three additional washes with D-PBS, samples were counterstained with or without DAPI (1:1000) and
793 mounted using Fluoromount-G Mounting Medium (Invitrogen). Cell death was analysed using CC3 and
794 DAPI markers by confocal microscopy with a 40×/1.3 NA objective. Maximum-intensity projections were
795 used to illustrate Flower protein localization and cell death in the cultures.

796 Secreted Flower particles were analysed by super-resolution SIM using a 63×/1.4 NA objective. SIM
797 imaging were performed on a Zeiss Elyra PS.1 microscopic SIM System with Zen 2010 software for
798 device control and high-resolution image processing. Images were acquired as z-stacks with 0.15-µm
799 intervals through the entire particles. Single-plane images were used to illustrate Flower protein
800 localization on the particles.

801

802 **Amyloid plaques extraction by laser capture dissection**

803 Freshly isolated brains from APP-transgenic mice were fixed in 4% PFA overnight and subsequently
804 processed for paraffin embedding. Fixed tissues were dehydrated through a graded ethanol series (70%,
805 80%, and 95% ethanol for 1.5 h each), followed by three washes in 100% ethanol (2 h each). Samples
806 were cleared in xylene (three times for 1.5 h), then infiltrated with paraffin wax at 60 °C (two rounds of
807 1.5 h each). Embedded tissues were oriented in molds and cooled at room temperature to solidify.

808 Paraffin blocks were sectioned at 5 µm thickness using a microtome. Sections were floated on a 63–
809 65 °C water bath to remove wrinkles, then mounted onto RNase-free PEN membrane-coated glass
810 slides (VWR, Cat. No. 76414-898) for laser microdissection (Leica). Slides were air-dried and stained
811 with Congo Red to label amyloid plaques and Hematoxylin to visualize cellular architecture prior to RNA
812 extraction.

813 Laser capture microdissection was performed using a Leica LMD system. Congo Red–positive amyloid
814 plaques were identified under fluorescence illumination and precisely cut using the UV laser.
815 Microdissected tissue fragments were collected directly into RNase-free microcentrifuge tube caps
816 containing lysis buffer for RNA isolation. To minimize RNA degradation, dissections were completed
817 within 1–2 h per slide, and slides were kept dry and protected from light. At least 100 ng total RNA was
818 collected per sample.

819 RNA was extracted from microdissected tissues using the RNeasy FFPE Kit (QIAGEN) following the
820 manufacturer's instructions. Briefly, tissues were lysed in PKD buffer, treated with Proteinase K,

821 incubated at 56 °C for 15 min followed by 80 °C for 15 min, and cooled on ice. Samples were centrifuged
822 at 20,000 × g for 15 min, and the supernatant was treated with DNase I. RNA was precipitated, bound
823 to an RNeasy MinElute spin column, washed, and eluted in RNase-free water. RNA quantity and purity
824 were assessed using a NanoDrop spectrophotometer.

825

826 **RNA isolation, cDNA synthesis and RT–qPCR**

827 Total RNA from cultured cells was extracted using TRIzol reagent (Thermo Fisher Scientific) according
828 to the manufacturer's protocol. Briefly, 5×10^6 cells were homogenized in 500 µl TRIzol, followed by the
829 addition of 100 µl chloroform. Samples were centrifuged at 12,000 × g for 15 min at 4 °C, and the
830 aqueous phase containing RNA was transferred to a fresh tube. RNA was precipitated with an equal
831 volume of 100% isopropanol, washed once with 75% ethanol, air-dried, and dissolved in DEPC-treated
832 H_2O.

833 For cDNA synthesis, 1 µg of total RNA was reverse-transcribed using the ABScript II cDNA First-Strand
834 Synthesis Kit (ABclonal) according to the manufacturer's instructions. The reaction mix contained
835 Random Primer Mix, 10 mM dNTPs, and ABScript II reverse transcriptase. Reactions were incubated
836 at 25 °C for 5 min, followed by 42 °C for 1 h, and terminated at 80 °C for 5 min. Real-time quantitative
837 PCR (RT–qPCR) was performed using Genious 2× SYBR Green Fast qPCR Mix (ABclonal) on a CFX96
838 Touch Real-Time PCR Detection System (Bio-Rad). Each reaction contained 10 ng of cDNA and gene-
839 specific primers targeting mFwe1, mFwe2, mFwe3, mFwe4, Caspase3, Bax, Bcl2, Gfap, Lcn2, C3,
840 Serping1, S100a10, Ptx3, Megf10, Mertk, Lrp1, and Abca1. GAPDH served as the internal control.
841 Gene expression was normalized to GAPDH using the ΔCt method, and relative expression was
842 calculated by the ΔΔCt method.

843

844 **Oligonucleotides**

845 Quantitative PCR (qPCR) was performed using gene-specific primers designed for mouse Flower
846 isoforms (mFwe1–4), apoptosis-related genes, astrocytic markers, inflammatory genes, and lipid
847 metabolism-related genes. Primer sequences were as follows: For mFwe1, forward 5′-
848 ACTGACTCATCCAATAACAGG-3′ and reverse 5′-ACCATGCCTACACATACATTAG-3′; for mFwe2,
849 forward 5′-GCCATTTCTTATGCTCGGAT-3′ and reverse 5′-GCCATTTAACAGAGCTGACA-3′; for
850 mFwe3, forward 5′-GTCTTCTACTGCGGGCAT-3′ and reverse 5′-AGAGGGAAATGGTGTTTCTG-3′; for
851 mFwe4, forward 5′-TTGCTAAATCCTGGGTGTCC-3′ and reverse 5′-TGTTCAGAGGGTGGATAGTG-3′.
852 For apoptosis-related genes, primers were: Bax, forward 5′-CTACAGGGTTTCATCCAG-3′ and reverse
853 5′-TATTGCTGTCCAGTTCATCT-3′; Bcl2, forward 5′-TACCTGAACCGGCATCT-3′ and reverse 5′-
854 CAGCCAGGAGAAATCAAACA-3′; and Casp3, forward 5′-GGCTTGCCAGAAGATAC-3′ and reverse 5′-
855 CTCCAGGAATAGTAACCAG-3′. For astrocytic and inflammatory markers, primers were: Gfap, forward
856 5′-AAATTGCTGGAGGGCGAAGAA-3′ and reverse 5′-TGTGAGCCTTTTGAGAGGTCTT-3′; Lcn2,
857 forward 5′-AATGTCACCTCCATCCTGGTC-3′ and reverse 5′-GCCACTTGCACATTGTAGCTC-3′; C3,
858 forward 5′-TCCCAGCTACTAGTGCTACTG-3′ and reverse 5′-CAGTACGATGGTCTCTTCGC-3′;

Serping1, forward 5′-AGTGCCCATGATGAGTAGCG-3′ and reverse 5′-CACGGGTACCACGATCACAA-3′; S100a10, forward 5′-GACAAAGGAGGACCTGAGAGTG-3′ and reverse 5′-CTCTGGAAGCCCACTTTGCCAT-3′; and Ptx3, forward 5′-CAATGGACTTCATCCCACCGA-3′ and reverse 5′-ACAGCTTGTCCCACTCCGA-3′. For phagocytosis- and lipid metabolism-related genes, primers were: Megf10, forward 5′-CAGCGCCTATGATGGGGAAT-3′ and reverse 5′-CACTGCCCCGAGATATGGTC-3′; Mertk, forward 5′-CGCTCAGACAATGGGTCGT-3′ and reverse 5′-AAGGCTGTGTTTCTGGTGACA-3′; Lrp1, forward 5′-GTATTGAGCGGTCTCGCCTT-3′ and reverse 5′-CATCCGAGCATCACACCAGT-3′; and Abca1, forward 5′-TAGCAGCACCGTGTCTTGTC-3′ and reverse 5′-GCGTGTCACTTTCATGGTCG-3′. Gapdh was used as the internal reference gene, with forward primer 5′-GTATGTCGTGGAGTCTACTG-3′ and reverse primer 5′-TATTTCTCGTGGTTCACACC-3′.

Flower topology experiments

To investigate the membrane topology of the Flower protein, mFwe1 and mFwe2 fusion constructs were generated by incorporating the ratiometric pH-sensitive fluorophore pHluorin2. The pHluorin2 tag was fused to either the N- or C-terminus of the Flower protein. Additionally, syb2-pHluorin2 and cytosolic pHluorin2 constructs were used as internal controls. WT astrocytes were transfected individually with each pHluorin2 construct. Following transfection, cells were plated onto glass coverslips and allowed to adhere for 24 h. Fluorescence measurements were acquired using a confocal microscope (LSM 780, Zeiss) equipped with a 40× objective. Images were recorded in 0.5 Hz. Fluorescence was monitored before and after perfusion with 200 μM carbonyl cyanide m-chlorophenyl hydrazone (CCCP, Sigma), using excitation wavelengths of 405 nm and 488 nm. CCCP induces cytosolic acidification, which alters the fluorescent properties of pHluorin2. In acidic conditions, pHluorin2 exhibits a decrease in excitation at 395 nm and an increase at 475 nm.

Software and Statistical analysis

Image analysis was performed using Fiji (RRID: SCR_002285). Statistical analyses were conducted using SigmaPlot v14.5 and Igor Pro 6.37. Flow cytometry data were analyzed with FlowJo. qPCR data were processed using Bio-Rad CFX Manager software. Figures were prepared using BioRender and CorelDRAW Graphics Suite. The specific statistical tests used are indicated in each figure legend. Student's t-test, one-way ANOVA or two-way ANOVA were applied, as appropriate, followed by Tukey's, Dunn's or Holm–Sidak post hoc tests for multiple comparisons to assess statistically significant differences between groups. All values are presented as mean ± SEM from independent experiments.

Data Availability

All data supporting the findings of this study are available within the paper and its Supplementary Information file. Raw data and statistical analysis data are provided as a source data file.

896 **Figure Legend**

897 **Figure 1. Flower-mediated regulation of cell fitness in primary astrocytes. (A)** Schematic
898 representation of mouse Flower isoforms (mFwe1–4), illustrating comparable exon and intron structures
899 across splice variants. **(B)** Schematic of the experimental procedure. Primary astrocytes were isolated
900 from Flower KO pups and cultured for 9–12 days before electroporation. Individual Flower isoforms
901 were introduced into astrocytes via electroporation. Transfected cells were then mixed at a 1:1 ratio to
902 establish homotypic and heterotypic co-cultures. After 24 h of co-culture in a 6-well plate, cells were
903 fixed and stained for cell death markers. Confocal imaging was used to assess cell death resulting from
904 Flower-mediated cell selection. **(C)** Confocal images of primary astrocytes expressing the "win" Flower
905 isoform (yellow) co-cultured with astrocytes expressing the "lose" isoform (cyan). Cell-cell contacts
906 between isoform-expressing cells were analysed after 24 h. Cultures were fixed and stained with
907 cleaved caspase-3 (CC3; magenta) to mark apoptotic cells, while DAPI staining (blue), applied before
908 fixation to identify non-intact cells or fragmented nuclei indicative of late apoptosis. Scale bar, 20 µm.
909 White arrows indicate CC3+ apoptotic cells, and green arrows point to fragmented DAPI+ nuclei. **(D)**
910 Quantification of cell death in homotypic pairwise win-win, lose-lose, and heterotypic win-lose co-
911 cultures. Cell death was assessed based on CC3 and DAPI staining in each co-culture (n= 500-1200
912 cell contacts; N=3 independent mouse preparations). Each data point represents the mean of the
913 indicated combinations: Win+Win (mFwe2+mFwe2, mFwe2+mFwe4, mFwe4+mFwe4), Lose+Lose
914 (mFwe1+mFwe1, mFwe1+mFwe3), and Win+Lose (mFwe2+mFwe1, mFwe2+mFwe3,
915 mFwe4+mFwe1, mFwe4+mFwe3). **(E)** Quantification of cell death in individual isoform-expressing cells
916 in heterotypic win-lose pairwise co-cultures (n= 260-360 cell contacts; N=2 independent mouse
917 preparations). **(F)** Confocal images of mouse primary Flower KO astrocytes expressing the human
918 Flower "win" isoform 4 (yellow) co-cultured with astrocytes expressing the human "lose" isoform 3
919 (cyan). Cell-cell contacts between hFwe 3- and hFwe 4-expressing cells were analysed after 24 h.
920 Cultures were fixed and stained with CC3 (magenta) to identify apoptotic cells. DAPI staining (blue),
921 applied before fixation to define non-intact cells or fragmented nuclei indicative of late apoptosis. Scale
922 bar, 20 µm. **(G)** Quantification of cell survival in co-cultures. Dead cells were counted based on CC3
923 and DAPI staining (N = 3 independent experiments; n= 430-760 cell contacts were analysed). Each
924 data point represents the indicated combination: Win+Win (hFwe4 + hFwe4), Lose+Lose (hFwe3 +
925 hFwe3), and Win+Lose (mean of reciprocal fluorophore labeling, hFwe4-mCherry + hFwe3-mTFP and
926 hFwe4-mTFP + hFwe3-mCherry). Statistical significance was determined by one-way ANOVA followed
927 by Holm-Sidak post hoc test for multiple comparisons (***$p < 0.001$). **(H)** Quantification of cell death in
928 win-lose co-culture from **G**. Data are presented as mean ± SEM. Statistical significance was determined
929 using Student's t-test: *$p < 0.05$, **$p < 0.01$, ***$p < 0.001$.

930

931 **Figure 2. N- and C-termini of Flower proteins are localized on the intracellular side of mouse**
932 **primary astrocytes. (A)** Quantitative RT-PCR analysis of Flower mRNA expression of all Flower
933 isoforms in WT astrocytes. (N = 3). Data are presented as mean ± SEM. Statistical significance was
934 determined by one-way ANOVA followed by Holm-Sidak post hoc test for multiple comparisons:

935 *p < 0.05 and ***p < 0.001. **(B)** Left: SIM images of WT astrocytes transfected with Flag–mFwe1–HA or
936 Flag–mFwe2–HA. Cells were fixed and stained with anti-Flag antibody. White arrows indicate Flower
937 localization at the plasma membrane. Scale bar: 10 µm. Right: Schematic illustrating the two potential
938 membrane topologies of Flower on intracellular vesicles in astrocytes. **(C-H)** WT astrocytes were
939 transfected with pH-sensitive pHluorin2 constructs to evaluate the orientation of the N- and C-termini of
940 Flower proteins (mFwe1 and mFwe2) in relation to the vesicle lumen or cytoplasm. Cytosolic-pHluorin2
941 and Syb2-pHluorin2 were used as internal controls, representing known pHluorin2 localization in the
942 cytoplasm and vesicle lumen, respectively. Ionophore CCCP was applied to transfected cells to induce
943 pH changes, while DMSO served as the control vehicle. Live-cell confocal imaging was used to record
944 ratiometric changes by sequential excitation at 405 nm and 488 nm. Construct details and sample sizes
945 are as follows: cytosolic-pHluorin2 (DMSO, n = 19 cells; CCCP, n = 32 cells), mFwe1-pHluorin2 (DMSO,
946 n = 34; CCCP, n = 57), pHluorin2-mFwe1 (DMSO, n = 29; CCCP, n = 31), Syb2-pHluorin2 (DMSO, n =
947 50; CCCP, n = 54), mFwe2-pHluorin2 (DMSO, n = 37; CCCP, n = 71), and pHluorin2-mFwe2 (DMSO,
948 n = 42; CCCP, n = 60). N = 3 independent experiments.

949

950 **Figure 3. Extracellular vesicle–associated Flower mediates cellular fitness signaling.**
951 **(A)** Left: Experimental workflow for extracellular vesicle (EV) isolation. Astrocytes were cultured for two
952 weeks following cortical isolation, and culture supernatants were collected for EV pelleting via
953 ultracentrifugation. Right: Western blot analysis of EV lysates from WT astrocyte cultures transfected
954 with mFwe1 or mFwe2. Ten micrograms of EV protein were loaded per lane. Anti-CD63 antibody was
955 used to identify the EV population. **(B)** SIM images of EVs derived from astrocytes expressing Flag-
956 mFwe1-HA or Flag-mFwe2-HA (right). Pelleted EVs were fixed and stained with anti-Flag (cyan), anti-
957 HA (yellow), and DiD (magenta) to visualize N- and C-terminal fragments and their association with EV
958 membranes. Schematic representations of Flower constructs ("win" Fwe2 and "lose" Fwe1) used in this
959 study are shown (top). Scale bar, 1 µm. **(C)** Representative TEM images of EVs isolated from WT
960 astrocyte culture supernatants. EVs were deposited onto pioloform-coated copper grids and
961 immunogold-labeled with an anti-Pan-Flower primary antibody and a goat anti-rabbit secondary
962 antibody conjugated to 10nm gold particles. Scale bar, 100 nm. (WT n_{EVs}=10, N_{Pups}=6). **(D)** TEM images
963 of EVs isolated from WT astrocytes expressing Flag-mFwe2-HA. EVs were immunogold-labeled using
964 anti-HA antibody and detected with a goat anti-rat secondary antibody conjugated to 10 nm gold
965 particles (top). Co-labeling with anti-Flag and anti-HA antibodies was detected using goat anti-mouse
966 (6 nm) and goat anti-rat (10 nm) gold-conjugated secondary antibodies, respectively (bottom). Scale
967 bar, 100 nm. (anti-HA, n_{EVs}=14; anti-Flag/anti-HA, $n_{Evs=}$10; N_{Pups}=6). **(E)** Quantification of gold particle
968 numbers associated with immunolabeled EVs shown in **C** and **D**. Data are presented as mean ± SD.
969 (WT n_{EVs}=10; anti-HA, n_{EVs}=14; anti-Flag/anti-HA, $n_{Evs=}$10; N_{Pups}=6). **(F)** Size distribution analysis of
970 immunogold-labeled EVs shown in **C** and **D**. Data are presented as mean ± SD. (WT n_{EVs}=10, N_{Pups}=6).
971 **(G)** Western blot analysis of secreted mFwe1 and mFwe2 in EV fractions isolated from WT astrocytes
972 transfected with Flower constructs. Ten micrograms of EV protein were loaded per lane. Membranes
973 were sequentially probed with anti-Flag and anti-HA. **(H)** Quantification of relative levels of secreted
974 Fwe2 compared to Fwe1 from (**G**) (N = 3 independent experiments). Data are presented as mean ± SD.

975 Statistical significance was determined using Student's t-test: **p < 0.01. **(I)** Experimental workflow
976 assessing the effect of Flower-containing EVs on cellular fitness (left). EVs isolated from WT, mFwe1-,
977 or mFwe2-expressing astrocytes were applied to unfit cell populations. Representative confocal images
978 of mFwe1-expressing unfit cells treated with EVs derived from WT, mFwe1-, or mFwe2-overexpressing
979 astrocytes (right). Approximately 10 µg of EVs were applied to 100,000 recipient cells seeded on 12.5-
980 mm coverslips in 24-well plates. After 24 h, cells were fixed and stained with anti-CC3 to label apoptotic
981 cells. Scale bar, 50 µm. **(J)** Quantification of apoptotic cells from (H) (control n = 616; WT EVs n = 665;
982 mFwe1 EVs n = 687; mFwe2 EVs n = 917; N = 3). Data are presented as mean ± SEM. Statistical
983 significance: one-way ANOVA with Tukey's post hoc test, *p < 0.001.
984

985 **Figure 4. The Flower N-terminus acts as an extrinsic pro-apoptotic ligand antagonized by the C-**
986 **terminal domain. (A)** Schematic representation of putative signaling domains located at the N-terminus,
987 C-terminus, and Exon 3 region of the full-length mFwe2 sequence. **(B-J)** Cell fitness assays were
988 performed using Flower KO astrocytes expressing the indicated Flower isoforms to generate fit or unfit
989 cell populations. Cells were treated with synthesized Flower N-terminal, C-terminal, or exon 3-derived
990 peptides, or co-overexpressed with the corresponding truncated Flower constructs for cell-death rescue
991 experiments. Cultures were fixed 24 h after treatment or co-culture, and cell death was assessed based
992 on DAPI staining or CC3+ immunostaining. **(B)** Confocal images of cells expressing specific Flower
993 signaling domains (yellow) localized at the plasma membrane (-TM) with extracellular orientation, co-
994 cultured with unfit mFwe1-mTFP-expressing “lose” cell populations (cyan). Cultures were stained with
995 DAPI before fixation and anti-CC3 antibody (magenta) after fixation to analyse positively stained dead
996 cells. Scale bar, 20 µm. **(C)** Quantification of overall cell viability in co-cultures of Flower KO astrocytes
997 expressing individual signaling domains (N terminus-, exon3- or C terminus-TM) with either fit (mFwe2)
998 or unfit (mFwe1) cell populations (n = 255–342 cells per group; N = 3 independent experiments).
999 Statistical significance was determined by two-way ANOVA followed by Holm-Sidak post hoc test for
1000 multiple comparisons: ***p < 0.001. **(D)** Detailed analysis of cell death in co-cultures of KO astrocytes
1001 expressing the N-terminal Flower construct (Flower N-term-TM) and mFwe1-expressing unfit cells, as
1002 shown in the first group of panel (**C**) (n = 307 cells; N = 3 independent experiments). Statistical
1003 significance was determined using Student's t-test: **p < 0.01. **(E)** Confocal images of synthetic Flower
1004 N-terminus peptides applied to mFwe1-expressing unfit cells. Cultures were fixed and stained as
1005 described. Control cells were treated with DMSO. Scale bar, 50 µm. **(F)** Synthetic Flower signal peptides
1006 affect cell fitness. Peptides representing three Flower domains were incubated with mFwe1- or mFwe2-
1007 expressing cells for 24 h, and cell death was quantified. Data represent >300 cells per condition from
1008 N = 3 independent experiments. Statistical significance was determined by one-way ANOVA followed
1009 by Tukey’s post hoc test (**p < 0.01, ***p < 0.001). **(G)** Dose-dependent effect of the Flower N-terminal
1010 peptide on apoptosis in unfit cells. mFwe1- and mFwe3-expressing cells were treated with 0.1, 1, or
1011 10 µg/ml of N-terminal peptide or DMSO control for 24 h. Cell death was quantified (n = 311–631 cells
1012 per condition; N = 3 independent experiments). Statistical significance was determined by one-way
1013 ANOVA with Tukey’s post hoc test (*p < 0.05, **p < 0.01, ***p < 0.001). **(H-I)** Role of the Flower C-
1014 terminus-TM peptide in rescuing cell death induced by the N-terminus peptide. mFwe1- and mFwe3-

1015 expressing unfit cells were treated with suspended Flower N-terminus peptide and transfected with or
1016 without the C terminus-TM construct. **(H)** Representative confocal images of mFwe1-expressing unfit
1017 astrocytes co-expressing the C-terminal-TM construct and treated with synthetic N-terminal peptide.
1018 Unfit cells without C-terminal-TM expression, treated with DMSO or N-terminal peptide, served as
1019 controls. Cells were fixed and stained with CC3 antibody to label apoptotic cells. Scale bar: 50 μm. **(I)**
1020 Quantification of dead cells following N-terminal peptide treatment, with or without co-expression of the
1021 C-terminal domain. mFwe1- and mFwe3-expressing cells were treated for 24 h, and cell death was
1022 quantified (n = 278–617 cells per condition; N = 3 independent experiments). Statistical significance
1023 was determined by two-way ANOVA followed by Holm-Sidak post hoc test for multiple comparisons:
1024 ***$p < 0.001$. **(J)** Quantitative RT-PCR analysis of Flower signal peptide-mediated cell death. KO
1025 astrocytes were transfected with mFwe1 to generate unfit cells and treated with the N-terminus peptide,
1026 with or without rescue by overexpression of Flower C- or N-terminus constructs. Apoptosis-related
1027 genes (Caspase-3, Bax, and Bcl2) were analysed after 24 h (N = 3). Data are presented as mean ±
1028 SEM. Statistical significance was determined by two-way ANOVA followed by Holm-Sidak post hoc test
1029 for multiple comparisons: *$p < 0.05$ and **$p < 0.01$.

1030

1031 **Figure 5. Model of EV-mediated astrocyte fitness surveillance and distal cell elimination.**

1032 "Win" (mFwe2) astrocytes secrete specialized extracellular vesicles (EVs) displaying N-terminal "death"
1033 domains in an "extracellular-out" orientation. These EVs act as long-range signals that target "lose"
1034 (mFwe1) astrocytes, triggering a pro-apoptotic transcriptional program defined by *Bax* and *Caspase-3*
1035 induction. In contrast, the C-terminal domain (Fwe C-TM) functions as a competitive antagonist. By
1036 directly binding to the EV-derived N-terminal domain, the C-terminus physically neutralizes the pro-
1037 apoptotic signal. This binding-dependent interference protects "unfit" astrocytes from elimination.

1038

1039 **Figure 6. Flower is highly expressed in a subset of astrocytes near amyloid plaques in the**
1040 **neocortex.**

1041 **(A)** Analysis of microarray data from hippocampal specimens of AD patients with different disease
1042 severities and from controls (GSE1297)(Blalock *et al.*, 2004). Heatmap showing the correlation between
1043 CACFD1 expression and Braak stage or neurofibrillary tangle (NFT) score. Values are normalized to z-
1044 scores (sample value minus dataset mean divided by standard deviation). The heatmap was generated
1045 using Morpheus (https://software.broadinstitute.org/morpheus/); the color scale represents z-scores. **(B)**
1046 Relative CACFD1 expression across diagnostic groups. Lines indicate medians. $P < 0.05$ by two-tailed
1047 Kruskal–Wallis test. Control, n = 9; incipient AD, n = 7; moderate AD, n = 8; severe AD, n = 7. **(C)**
1048 Histological staining of post-mortem brain cortex from AD patients. Plaques are marked with black
1049 circles. Left: astrocytes stained with anti-GFAP antibody. Right: co-staining for Flower (blue) and
1050 astrocytes (brown). Black arrows indicate double-positive cells. Scale bar: 50 μm. **(D)** Confocal images
1051 of post-mortem brain cortex from AD patients. Flower (yellow) and GFAP (cyan) were stained to label
1052 Flower-expressing astrocytes. White arrows point to Flower-expressing astrocytes near plaques. **(E)**

Quantification of Flower-expressing astrocyte populations near plaques versus non-plaque areas from (**D**) (N = 3 donor; n = 45 images; n = 1096 cells). **(F)** RT–qPCR analysis of total Flower expression in cortices from APP transgenic mice compared with WT controls. Data are presented as fold change relative to WT cortex. Flower isoform transcripts were normalized to GAPDH. Flower isoforms were normalized to GAPDH (N = 2). **(G)** Left: Representative cortical section from an APP mouse stained with Congo Red to label amyloid plaques (red) and hematoxylin to label nuclei (blue). Plaque regions (red circles) and non-plaque regions (black circles) were microdissected for RT–qPCR analysis. Right: RT–qPCR analysis of Flower isoform expression in plaque- or non-plaque-associated regions of APP mouse cortex (N = 2). **(H-J)** Representative confocal images of the neocortex from APP mice. Amyloid plaques were labeled with Thioflavin-S (Thio-S) (cyan), and glial cells were stained with anti-GFAP (astrocytes) and anti-IBA1 (microglia). Scale bar: 50 µm. **(I-J)** Endogenous Flower was stained with anti-Flower antibody #C-1557 (magenta) along with glial markers (yellow). White arrows indicate Flower-expressing astrocytes near plaques. **(K)** Quantification of Flower-high-expressing astrocytes and microglia in plaque-associated regions compared to non-plaque areas, based on the total counted glial cells. Left: astrocytes; right: microglia, derived from images in (**I**) and (**J**) (N = 3 mice; n = 30 images; 1167 astrocytes and 967 microglia were analysed). Data are presented as mean ± SEM. Statistical significance was determined using Student's t-test: *p < 0.05, ***p < 0.001.

Figure 7. Flower "win" isoforms coordinate astrocyte fitness and Aβ clearance to promote neuroprotection. (A) Confocal images of transfected neuronal cultures treated with Aβ protofibrils-Alexa647. WT neuronal cultures were lentivirally infected at DIV1 with Flower-mScarlet I constructs (mFwe2-mScarlet I or C-terminal-mScarlet I) or a control mScarlet I vector (yellow). At DIV7, cultures were treated with or without Aβ protofibrils-Alexa647 (cyan). Neuronal cultures were fixed after 6 days and stained with CC3 antibody (magenta) to identify apoptotic cells. White arrows point to the translocated Flower C terminal protein. Scale bar, 50 µm. Right: schematic representation of the corresponding cultures and treatments shown on the left. **(B)** Quantification of CC3+ cell death from panel A. Data are presented as mean ± SEM. Statistical significance was determined using Student's t-test: **p < 0.01. **(C)** Flow cytometric analysis of Aβ protofibril uptake by glial populations. Neuronal cultures were trypsinized and analyzed for the proportion of Aβ-positive cells. WT vector control (white) and mFwe2-expressing cells (red) are shown (N = 3). **(D)** Quantification of Aβ-positive cell populations from (**C**). Data are presented as mean ± SEM. Statistical significance was determined using Student's t-test; **p < 0.01, ***p < 0.001. **(E)** Analysis of Aβ aggregate size in vector-transfected control (WT) and mFwe2-expressing cultures after 6 days. Data are presented as box-and-whisker plots. Statistical analysis was performed using one-way ANOVA followed by Dunn's post hoc test; ***p < 0.001 (N = 3). **(F)** Quantification of Flower C-terminal nuclear translocation from confocal images shown in (**A**). **(G)** Quantitative RT–PCR analysis of apoptosis-related genes in cells overexpressing the cytosolic Flower C terminus under N-terminal peptide–induced death signaling. WT astrocytes were transfected with mFwe1 alone or co-transfected with the cytosolic C-terminal fragment to assess protective effects in unfit cells. Cells were treated with the N-terminal peptide, and expression of apoptosis-related genes (Caspase-3, Bax, and Bcl2) was analyzed after 24 h (N = 3). Data are presented as mean ± SEM.

Statistical analysis was performed using two-way ANOVA followed by Holm–Šídák post hoc test; **$p < 0.01$, ***$p < 0.001$. **(H)** Model of Flower-mediated fitness surveillance and astrocyte-mediated neuroprotection. Schematic illustrating the bifurcated mechanism by which the Flower "win" isoform (mFwe2) coordinates astrocyte fitness and Aβ clearance. Left: In the absence of Flower-mediated selection, amyloid stress leads to widespread fitness loss and stochastic apoptosis, leaving the neural environment vulnerable. Right: Overexpression of mFwe2 reprograms the population: "win" astrocytes secrete Flower-positive EVs to eliminate distal, unfit "loser" cells while concurrently enhancing Aβ uptake. Internally, the C-terminal fragment translocates to the nucleus to repress Caspase-3 transcription, providing the cell-intrinsic survival necessary to maintain a protective astrocytic shield around plaques. Together, these pathways promote a robust state of tissue resilience in the AD brain.

1108 **Expanded View Figure Legend**

1109 **Figure EV1. Cleaved Flower fragments in astrocytes, related to Figure 3. (A)** Confocal images of
1110 cortical brain slices from APP-transgenic mice and postmortem human brain tissue from AD patients.
1111 Flower isoforms were detected using a C-terminal-specific Flower antibody (#C-1557). Arrows indicate
1112 Flower signal localized in the extracellular matrix. A white dashed circle marks a plaque in the human
1113 tissue. Scale bar, 20 µm. **(B-C)** Western blot analysis showing proteolytic cleavage of overexpressed
1114 Flower isoforms. Flower KO astrocytes were transfected with 3×Flag-mFwe-3×HA constructs,
1115 containing a Flag tag at the N-terminus and an HA tag at the C-terminus. Lysates from untransfected
1116 Flower KO astrocytes served as negative controls. GAPDH was used as a loading control (N = 3
1117 independent experiments). **(B)** Left: Blot probed with anti-Flag antibody to detect N-terminal fragments
1118 from all expressed isoforms. Right: Quantification of full-length and cleaved fragments. **(C)** Left: Blot
1119 probed with anti-HA antibody to detect C-terminal fragments. Right: Quantification of full-length and
1120 cleaved fragments. **(D)** Longer exposure of a separate blot from the same experiment, reprobed with
1121 anti-Pan-Flower antibody to confirm band identity.

1122

1123 **Figure EV2. Isoform-specific association of Flower with extracellular vesicles in astrocytes,**
1124 **related to Figure 3. (A)** SIM images of supernatant fractions collected from WT or mFwe2-pHluorin2-
1125 expressing astrocyte cultures. Pelleted fractions were deposited onto poly-ornithine-coated glass
1126 coverslips, fixed, and stained with a polyclonal Pan-Flower antibody recognizing both N- and C-termini,
1127 together with DiD to label lipid membranes. In mFwe2-overexpressing cultures, anti-GFP antibody was
1128 used to detect overexpressed Flower. Scale bar, 1 µm. **(B)** Quantification of co-localization between
1129 Flower-positive particles and the lipid dye DiD from (**A**). Statistical significance was determined using
1130 Student's t-test: $^{**}p < 0.01$. **(C)** Analysis of secreted Flower from overexpressing astrocytes shown in
1131 Fig. 3B. Supernatants from Flower KO astrocyte cultures transduced with 3×Flag-Flower-3×HA
1132 constructs were analysed by immunostaining with anti-Flag (N-terminal) and anti-HA (C-terminal)
1133 antibodies. Co-staining with a lipid dye assessed potential association with EVs. SIM was performed
1134 on supernatants from mFwe1- and mFwe2-expressing cells (N = 3; mFwe1: 5,330 particles; mFwe2:
1135 5,348 particles). Data are presented as mean ± SEM. Statistical significance was determined by one-
1136 way ANOVA followed by Tukey's post hoc test ($^{*}p < 0.05$, $^{**}p < 0.01$). **(D)** Particle analysis of EVs
1137 isolated from astrocyte cultures expressing GFP vector control, Flag-mFwe1-HA, or Flag-mFwe2-HA.
1138 Particle number and radius are shown. **(E)** Background control for immunogold labeling experiments
1139 shown in Fig. 3C and D. Immuno-labeling was done under the same conditions as described in Fig. 3C
1140 and D, without the application of a primary antibody to confirm the gold bead background. From left to
1141 right: electron micrographs of EVs immune-labeled with goat anti-rabbit (10 nm, GAR), goat anti-rat (10
1142 nm, GARat) and goat anti-mouse (6 nm, GAM) together with GAR (10 nm) are shown. Scale bar, 0.5
1143 µm. **(F)** Western blot analysis of secreted EV lysates from WT astrocyte cultures transfected with
1144 mFwe1 or mFwe2. Ten micrograms of EV protein were loaded per lane. The blot shown in Fig. 3G was
1145 stripped and sequentially reprobed with anti-Pan-Flower antibody (left). Anti-GAPDH antibody was used
1146 to assess EV purity (total astrocyte lysate included as a positive control) (right). **(G)** Primary mouse

astrocytes were transfected with either the "lose" isoform (mFwe1-mCherry or mFwe1-mTFP) or the "win" isoform (mRFP-mFwe2 or mFwe2-mTFP) to assess transfection efficiency. The number of fluorescent mFwe1$^+$ and mFwe2$^+$ cells was quantified from confocal images of separately cultured populations. N = 2 independent preparations; n = 84 cells for mFwe1, n = 101 cells for mFwe2. Statistical analysis was performed using Welch's t-test; two-tailed $P < 0.001$ (**). **(H)** Mean fluorescence intensity per cell from the same dataset as in (**G**), used to assess expression levels of mFwe1 and mFwe2. Red lines indicate median values. N = 2 independent preparations; n = 100 cells per group. Statistical comparison using the Mann–Whitney U test showed no significant difference.

Figure EV3. Flower-positive EVs represent a secretory population distinct from CD63$^+$ exosomes, related to Figure 3.

(A) SIM images of WT astrocytes co-transfected with CD63-pHuji together with mFwe1 or mFwe2 (3×Flag-Flower-3×HA). Cells were fixed 24 h after transfection and stained with anti-RFP, anti-Flag and anti-HA antibodies. Scale bar, 10 μm; inset: 1 μm. **(B)** Quantification of colocalization between CD63-phuji and Flag- or HA-tagged Flower isoforms from (**A**), expressed as Pearson's correlation coefficient. N = 4 pups for mFwe2 and N = 2 pups for mFwe1; n = 30 cells analyzed per group. **(C)** SIM images of WT astrocytes co-transfected with CD63-pHuji and mFwe2 (3×Flag–Fwe2–3×HA). EVs were harvested 3 days after transfection, fixed, and stained with anti-RFP, anti-Flag, and anti-HA antibodies under permeabilized or non-permeabilized conditions, as indicated. White arrows indicate CD63$^+$/mFwe$^+$ EVs. Scale bar: 1 μm. **(D)** Quantification of the percentage of CD63-positive puncta and mFwe-positive puncta under permeabilized and non-permeabilized conditions, analyzed from (**C**). HA single-positive, Flag single-positive, and double-positive puncta were defined as mFwe events. N = 4 pups for mFwe2 and N = 2 pups for mFwe1; n = 10 images analyzed per group. Upper Right: Schematic illustrating the transmembrane topologies of mFwe-bearing EVs and CD63-pHuji-labeled exosomes. **(E)** Representative electron micrographs of EVs used from (**C**). Co-immunogold labeling was performed using primary antibodies against pHuji (anti-mRFP), Flag, and HA, detected with goat anti-rabbit (6 nm), goat anti-mouse (15 nm), and goat anti-rat (10 nm) gold-conjugated secondary antibodies, respectively. Scale bar, 100 nm. **(F)** Size distribution analysis of immunogold-labeled EVs shown in (**E**). Data are presented as mean ± SD. Anti-CD63$^+$ EVs, n = 118; anti-HA-, anti-Flag-, or double-positive EVs (mFwe$^+$), n = 94; N = 4 pups. **(G)** Background control for immunogold labeling experiments shown in (**E**). Immuno-labeling was done under the same conditions as described in (**E**), without the application of primary antibodies to confirm the gold particle background. Scale bar, 0.2 μm. **(H)** Model of heterogeneous Flower-containing vesicle populations in astrocytes. Schematic illustrating the two primary fates of Flower protein during astrocyte secretion. (i) Surface-retained Flower: Following vesicle fusion, a population of Flower protein remains integrated into the plasma membrane. (ii) Secreted Flower-EVs: Flower is released within a distinct class of extracellular vesicles. In both populations, the N- and C-termini are oriented toward the extracellular space ("extracellular-out"), rendering them accessible for intercellular interactions.

1185 **Figure EV4. The N-terminal Flower domain does not induce cell death in fit cell populations,**
1186 **related to Figure 4. (A)** Schematic of constructs in which truncated Flower domains (N-terminus, Exon
1187 3, or C-terminus) were fused to a transmembrane (TM) domain for plasma membrane (PM) localization
1188 with extracellular orientation. An HA tag was placed at the N-terminus and mScarlet I at the C-terminus
1189 to assess membrane orientation. **(B)** Confocal images of Flower KO astrocytes expressing truncated
1190 Flower domains targeted to the PM. To verify surface expression, fixed, non-permeabilized cells were
1191 stained with anti-RFP-Alexa647 (magenta) and anti-HA (cyan). Scale bar, 50 µm. **(C)** Confocal images
1192 of Flower KO astrocytes expressing specific truncated Flower domains (yellow) co-cultured with fit
1193 mFwe2-mTFP-expressing "win" cells (cyan). Cultures were stained with DAPI before fixation and with
1194 anti-CC3 (magenta) after fixation to detect apoptotic cells. Maximum intensity projection images are
1195 shown. Scale bar, 20 µm.

1196

1197 **Figure EV5. Overexpression of the C-terminus Flower domain does not alter cell survival, related**
1198 **to Figure 4. (A)** Flower KO astrocytes were transfected with mFwe1 or mFwe3 to generate unfit cell
1199 populations. Co-transfection with the C-terminal Flower domain (C-term-TM) plasmid did not affect cell
1200 survival upon treatment with the control vehicle, DMSO. **(B)** Quantitative RT-PCR analysis of apoptosis-
1201 related genes in transfected and treated cells. N = 3 independent experiments. Data are presented as
1202 mean ± SEM. Statistical significance was determined using Student's t-test: ns refers to not significant.

1203

1204 **Figure EV6. SPR analysis showing interaction between the N- and C-terminal and N- and N-**
1205 **terminal domains of Flower, related to Figure 5. (A-B)** SPR binding analysis showing interaction of
1206 Flower N-terminal and C-terminal peptides with immobilized Flower C-terminal peptide (engineered with
1207 an N-terminal cysteine for immobilization). **(C-D)** SPR binding analysis showing interaction of Flower
1208 N-terminal and N-terminal peptide with immobilized Flower N-terminal peptide. Representative
1209 sensorgrams **(A, C)** and the corresponding quantification **(B, D)** demonstrate binding responses at
1210 increasing concentrations (15, 30, and 40 µM). Bar graph shows mean ± s.d. from three independent
1211 experiments. One-way ANOVA: $^{**}p < 0.01$, $^{***}p < 0.001$.

1212

1213 **Figure EV7. Overexpression of Flower upregulates genes associated with astrocyte reactivation**
1214 **and lipid transport in an Aβ protofibril environment, related to Figure 7.** WT astrocytes and
1215 astrocytes lentivirally infected with mFwe2 construct were co-cultured with Aβ protofibrils for six days.
1216 **(A-E)** RNA was isolated from each group and analyzed by quantitative RT–PCR for the indicated genes.
1217 The indicated genes are shown. **(F)** Quantitative RT–PCR analysis of apoptosis-related genes
1218 (*Caspase-3, Bax, and Bcl2*) (N = 2 independent experiments). Data are presented as mean ± SEM.

References

Alawar N, Schirra C, Rasuli R, Fecher-Trost C, Weins L, Meyer MR, Flockerzi V, Keller A, Dustin ML, Rettig J *et al* (2026) T-Cell-Derived Exosomes From Multi Core Granules Exhibit Superior Caspase-3-Mediated Tumor-Suppressive Activity Compared to Those From Multivesicular Bodies. *J Extracell Vesicles* 15: e70239

Blalock EM, Geddes JW, Chen KC, Porter NM, Markesbery WR, Landfield PW (2004) Incipient Alzheimer's disease: microarray correlation analyses reveal major transcriptional and tumor suppressor responses. *Proc Natl Acad Sci U S A* 101: 2173-2178

Brose N, Neher E (2009) Flowers for synaptic endocytosis. *Cell* 138: 836-837

Chang HF, Mannebach S, Beck A, Ravichandran K, Krause E, Frohnweiler K, Fecher-Trost C, Schirra C, Pattu V, Flockerzi V *et al* (2018) Cytotoxic granule endocytosis depends on the Flower protein. *J Cell Biol* 217: 667-683

Chaudhuri AD, Dastgheyb RM, Yoo SW, Trout A, Talbot CC, Jr., Hao H, Witwer KW, Haughey NJ (2018) TNFalpha and IL-1beta modify the miRNA cargo of astrocyte shed extracellular vesicles to regulate neurotrophic signaling in neurons. *Cell Death Dis* 9: 363

Cheng J, Liao Y, Xiao L, Wu R, Zhao S, Chen H, Hou B, Zhang X, Liang C, Xu Y *et al* (2017) Autophagy regulates MAVS signaling activation in a phosphorylation-dependent manner in microglia. *Cell Death Differ* 24: 276-287

Chipuk JE, Green DR (2008) How do BCL-2 proteins induce mitochondrial outer membrane permeabilization? *Trends Cell Biol* 18: 157-164

Cho TJ, Hackley VA (2010) Fractionation and characterization of gold nanoparticles in aqueous solution: asymmetric-flow field flow fractionation with MALS, DLS, and UV-Vis detection. *Anal Bioanal Chem* 398: 2003-2018

Coelho DS, Moreno E (2019) Emerging links between cell competition and Alzheimer's disease. *J Cell Sci* 132

Condello C, Yuan P, Schain A, Grutzendler J (2015) Microglia constitute a barrier that prevents neurotoxic protofibrillar Abeta42 hotspots around plaques. *Nat Commun* 6: 6176

Costa-Rodrigues C, Couceiro J, Moreno E (2021) Cell competition from development to neurodegeneration. *Dis Model Mech* 14

Dai DL, Li M, Lee EB (2023) Human Alzheimer's disease reactive astrocytes exhibit a loss of homeostastic gene expression. *Acta Neuropathol Commun* 11: 127

Delbridge AR, Grabow S, Strasser A, Vaux DL (2016) Thirty years of BCL-2: translating cell death discoveries into novel cancer therapies. *Nat Rev Cancer* 16: 99-109

Gogna R, Shee K, Moreno E (2015) Cell Competition During Growth and Regeneration. *Annu Rev Genet* 49: 697-718

Gomez-Arboledas A, Davila JC, Sanchez-Mejias E, Navarro V, Nunez-Diaz C, Sanchez-Varo R, Sanchez-Mico MV, Trujillo-Estrada L, Fernandez-Valenzuela JJ, Vizuete M *et al* (2018) Phagocytic clearance of presynaptic dystrophies by reactive astrocytes in Alzheimer's disease. *Glia* 66: 637-653

Jiwaji Z, Tiwari SS, Aviles-Reyes RX, Hooley M, Hampton D, Torvell M, Johnson DA, McQueen J, Baxter P, Sabari-Sankar K *et al* (2022) Reactive astrocytes acquire neuroprotective as well as deleterious signatures in response to Tau and Ass pathology. *Nat Commun* 13: 135

Kalkavan H, Green DR (2018) MOMP, cell suicide as a BCL-2 family business. *Cell Death Differ* 25: 46-55

Kannan S, Sutphin RM, Hall MG, Golfman LS, Fang W, Nolo RM, Akers LJ, Hammitt RA, McMurray JS, Kornblau SM *et al* (2013) Notch activation inhibits AML growth and survival: a potential therapeutic approach. *J Exp Med* 210: 321-337

Kim H, Leng K, Park J, Sorets AG, Kim S, Shostak A, Embalabala RJ, Mlouk K, Katdare KA, Rose IVL *et al* (2022) Reactive astrocytes transduce inflammation in a blood-brain barrier model through a TNF-STAT3 signaling axis and secretion of alpha 1-antichymotrypsin. *Nat Commun* 13: 6581

Kuo SP, Trussell LO (2009) A new ion channel blooms at the synapse. *Neuron* 63: 566-567

Levayer R, Dupont C, Moreno E (2016) Tissue Crowding Induces Caspase-Dependent Competition for Space. *Curr Biol* 26: 670-677

Li TN, Chen YJ, Lu TY, Wang YT, Lin HC, Yao CK (2020a) A positive feedback loop between Flower and PI(4,5)P(2) at periactive zones controls bulk endocytosis in Drosophila. *Elife* 9

Li Z, Moniruzzaman M, Dastgheyb RM, Yoo SW, Wang M, Hao H, Liu J, Casaccia P, Nogueras-Ortiz C, Kapogiannis D *et al* (2020b) Astrocytes deliver CK1 to neurons via extracellular vesicles in response to inflammation promoting the translation and amyloidogenic processing of APP. *J Extracell Vesicles* 10: e12035

Lines J, Baraibar AM, Fang C, Martin ED, Aguilar J, Lee MK, Araque A, Kofuji P (2022) Astrocyte-neuronal network interplay is disrupted in Alzheimer's disease mice. *Glia* 70: 368-378

Liu L, Feng D, Chen G, Chen M, Zheng Q, Song P, Ma Q, Zhu C, Wang R, Qi W *et al* (2012) Mitochondrial outer-membrane protein FUNDC1 mediates hypoxia-induced mitophagy in mammalian cells. *Nat Cell Biol* 14: 177-185

Madan E, Gogna R, Moreno E (2018) Cell competition in development: information from flies and vertebrates. *Curr Opin Cell Biol* 55: 150-157

Madan E, Peixoto ML, Dimitrion P, Eubank TD, Yekelchyk M, Talukdar S, Fisher PB, Mi QS, Moreno E, Gogna R (2020) Cell Competition Boosts Clonal Evolution and Hypoxic Selection in Cancer. *Trends Cell Biol* 30: 967-978

Madan E, Pelham CJ, Nagane M, Parker TM, Canas-Marques R, Fazio K, Shaik K, Yuan Y, Henriques V, Galzerano A *et al* (2019) Flower isoforms promote competitive growth in cancer. *Nature* 572: 260-264

Maddika S, Ande SR, Panigrahi S, Paranjothy T, Weglarczyk K, Zuse A, Eshraghi M, Manda KD, Wiechec E, Los M (2007) Cell survival, cell death and cell cycle pathways are interconnected: implications for cancer therapy. *Drug Resist Updat* 10: 13-29

Marques-Reis M, Moreno E (2021) Role of cell competition in ageing. *Dev Biol* 476: 79-87

Merino MM, Levayer R, Moreno E (2016) Survival of the Fittest: Essential Roles of Cell Competition in Development, Aging, and Cancer. *Trends Cell Biol* 26: 776-788

Merino MM, Rhiner C, Lopez-Gay JM, Buechel D, Hauert B, Moreno E (2015) Elimination of unfit cells maintains tissue health and prolongs lifespan. *Cell* 160: 461-476

Merino MM, Rhiner C, Portela M, Moreno E (2013) "Fitness fingerprints" mediate physiological culling of unwanted neurons in Drosophila. *Curr Biol* 23: 1300-1309

Merrifield RB (1963) Solid Phase Peptide Synthesis. I. The Synthesis of a Tetrapeptide. *Journal of the American Chemical Society* 85: 2149-2154

Moonen S, Koper MJ, Van Schoor E, Schaeverbeke JM, Vandenberghe R, von Arnim CAF, Tousseyn T, De Strooper B, Thal DR (2023) Pyroptosis in Alzheimer's disease: cell type-specific activation in microglia, astrocytes and neurons. *Acta Neuropathol* 145: 175-195

Moreno E, Fernandez-Marrero Y, Meyer P, Rhiner C (2015) Brain regeneration in Drosophila involves comparison of neuronal fitness. *Curr Biol* 25: 955-963

Ngo JM, Williams JK, Zhang C, Saleh AH, Liu XM, Ma L, Schekman R (2025) Extracellular Vesicles and Cellular Homeostasis. *Annu Rev Biochem* 94: 587-609

Parker T, Madan E, Gupta K, Moreno E, Gogna R (2020) Cell Competition Spurs Selection of Aggressive Cancer Cells. *Trends Cancer* 6: 732-736

Parker TM, Gupta K, Palma AM, Yekelchyk M, Fisher PB, Grossman SR, Won KJ, Madan E, Moreno E, Gogna R (2021) Cell competition in intratumoral and tumor microenvironment interactions. *EMBO J* 40: e107271

Patani R, Hardingham GE, Liddelow SA (2023) Functional roles of reactive astrocytes in neuroinflammation and neurodegeneration. *Nat Rev Neurol* 19: 395-409

Patel MR, Weaver AM (2021) Astrocyte-derived small extracellular vesicles promote synapse formation via fibulin-2-mediated TGF-beta signaling. *Cell Rep* 34: 108829

Petrova E, Lopez-Gay JM, Rhiner C, Moreno E (2012) Flower-deficient mice have reduced susceptibility to skin papilloma formation. *Dis Model Mech* 5: 553-561

Radde R, Bolmont T, Kaeser SA, Coomaraswamy J, Lindau D, Stoltze L, Calhoun ME, Jaggi F, Wolburg H, Gengler S *et al* (2006) Abeta42-driven cerebral amyloidosis in transgenic mice reveals early and robust pathology. *EMBO Rep* 7: 940-946

Ravichandran K, Schirra C, Urbansky K, Tu SM, Alawar N, Mannebach S, Krause E, Stevens D, Lancaster CRD, Flockerzi V *et al* (2024) Required minimal protein domain of flower for synaptobrevin2 endocytosis in cytotoxic T cells. *Cell Mol Life Sci* 82: 8

Rhiner C, Lopez-Gay JM, Soldini D, Casas-Tinto S, Martin FA, Lombardia L, Moreno E (2010) Flower forms an extracellular code that reveals the fitness of a cell to its neighbors in Drosophila. *Dev Cell* 18: 985-998

Rudd JC, Smits JPH, Kuwong PT, Johnson RE, Monga LMN, van Vlijmen-Willems I, Porter GL, Halloran PO, Sharma K, Schmidt KN *et al* (2025) Flower dependent trafficking of lamellar bodies facilitates maturation of the epidermal barrier. *Nat Commun* 16: 6892

Sanchez-Mico MV, Jimenez S, Gomez-Arboledas A, Munoz-Castro C, Romero-Molina C, Navarro V, Sanchez-Mejias E, Nunez-Diaz C, Sanchez-Varo R, Galea E *et al* (2021) Amyloid-beta impairs the phagocytosis of dystrophic synapses by astrocytes in Alzheimer's disease. *Glia* 69: 997-1011

Sandberg A, Luheshi LM, Sollvander S, Pereira de Barros T, Macao B, Knowles TP, Biverstal H, Lendel C, Ekholm-Petterson F, Dubnovitsky A *et al* (2010) Stabilization of neurotoxic Alzheimer amyloid-beta oligomers by protein engineering. *Proc Natl Acad Sci U S A* 107: 15595-15600

Schindelin J, Arganda-Carreras I, Frise E, Kaynig V, Longair M, Pietzsch T, Preibisch S, Rueden C, Saalfeld S, Schmid B *et al* (2012) Fiji: an open-source platform for biological-image analysis. *Nat Methods* 9: 676-682

Schnatz A, Muller C, Brahmer A, Kramer-Albers EM (2021) Extracellular Vesicles in neural cell interaction and CNS homeostasis. *FASEB Bioadv* 3: 577-592

Seidenthal M, Redzovic J, Liewald JF, Rentsch D, Shapiguzov S, Schuh N, Rosenkranz N, Eimer S, Gottschalk A (2025) Flower/FLWR-1 regulates neuronal activity via the plasma membrane Ca(2+) ATPase to promote recycling of synaptic vesicles. *Elife* 13

Sollvander S, Nikitidou E, Brolin R, Soderberg L, Sehlin D, Lannfelt L, Erlandsson A (2016) Accumulation of amyloid-beta by astrocytes result in enlarged endosomes and microvesicle-induced apoptosis of neurons. *Mol Neurodegener* 11: 38

Verweij FJ, Bebelman MP, Jimenez CR, Garcia-Vallejo JJ, Janssen H, Neefjes J, Knol JC, de Goeij-de Haas R, Piersma SR, Baglio SR *et al* (2018) Quantifying exosome secretion from single cells reveals a modulatory role for GPCR signaling. *J Cell Biol* 217: 1129-1142

Vousden KH, Prives C (2009) Blinded by the Light: The Growing Complexity of p53. *Cell* 137: 413-431

Xie JM, Li B, Yu HP, Gao QG, Li W, Wu HR, Qin ZH (2014) TIGAR has a dual role in cancer cell survival through regulating apoptosis and autophagy. *Cancer Res* 74: 5127-5138

Xue L, Zhang Z, McNeil BD, Luo F, Wu XS, Sheng J, Shin W, Wu LG (2012) Voltage-dependent calcium channels at the plasma membrane, but not vesicular channels, couple exocytosis to endocytosis. *Cell Rep* 1: 632-638

Yao CK, Lin YQ, Ly CV, Ohyama T, Haueter CM, Moiseenkova-Bell VY, Wensel TG, Bellen HJ (2009) A synaptic vesicle-associated Ca2+ channel promotes endocytosis and couples exocytosis to endocytosis. *Cell* 138: 947-960

Yao CK, Liu YT, Lee IC, Wang YT, Wu PY (2017) A Ca2+ channel differentially regulates Clathrin-mediated and activity-dependent bulk endocytosis. *PLoS Biol* 15: e2000931

Yekelchyk M, Madan E, Wilhelm J, Short KR, Palma AM, Liao L, Camacho D, Nkadori E, Winters MT, Rice ES *et al* (2021) Flower lose, a cell fitness marker, predicts COVID-19 prognosis. *EMBO Mol Med* 13: e13714

You Y, Borgmann K, Edara VV, Stacy S, Ghorpade A, Ikezu T (2020) Activated human astrocyte-derived extracellular vesicles modulate neuronal uptake, differentiation and firing. *J Extracell Vesicles* 9: 1706801

ACKNOWLEDGEMENTS

This work was supported by grants from the Deutsche Forschungsgemeinschaft (DFG), collaborative research center SFB894 (ID number 157660137), subproject A10 (to H.-F.C. and E.K.), and A14 (to V.F.) and FL153/10-2 (to V.F.), and the University of Saarland (HOMFORexzellent 2020, NanoBioMed Young Investigator Grant 2020, and HOMFOR Anschubfinanzierung 2025 to H.-F.C.). The surface plasmon resonance instrument was acquired for the Center for Molecular Signaling (PZMS) according to Art. §91b GG (SL1369001; INST 256/548-1). Part of the laser capture microdissection equipment was funded by the German Research Foundation (DFG; ID number 447452855; INST 256/541-1). Furthermore, we thank Keerthana Ravichandran, Margarete Klose, Anja Bergsträßer, Nicole Rothgerber, Katrin Sandmeier, Andrea Schottek and Christine Wesely for their excellent technical assistance.

AUTHOR CONTRIBUTIONS

H.-F.C. conceived and supervised the study. S.-M.T. performed all cellular fitness assays, molecular biology experiments, and tissue staining analyses. C.-H.L. and Y.S. assisted with neuronal culture preparation. L.Y. carried out AD human brain tissue sectioning and staining. J.H. performed laser microdissection of brain tissue. M.J. synthesized the peptides. C.S. performed EM analysis A.C. and S.R. carried out the SPR analysis. A.A. and D.Y. performed particle size analysis. W.J.S.-S. provided postmortem AD brain tissue. C:-A.Y. conducted Flower gene expression analysis in AD cohorts. V.F. generated the Flower antibodies and Flower-gene-deficient mice. H.-F.C. and E.K. secured funding for the project. L.Y. and C.-K.Y. and C. S. contributed essential intellectual input to the study. C.-K.Y., C.S. and V.F. critically reviewed the manuscript. H.-F.C. wrote the manuscript with input from all authors. All authors reviewed and approved the final version of the manuscript.

COMPETING INTERESTS

The authors declare no competing interests.

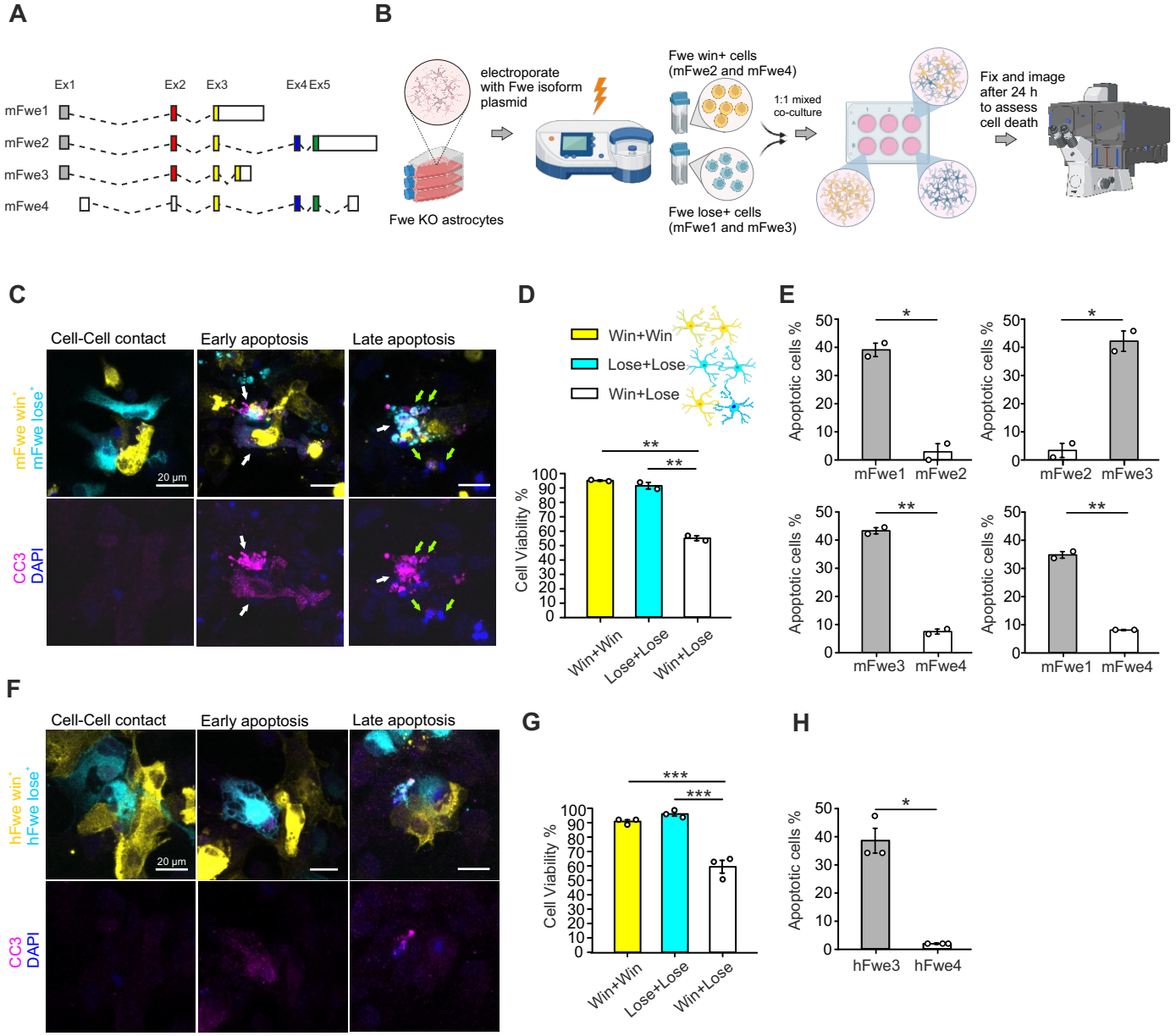
A
Ex1
Ex2
Ex3
Ex4 Ex5
mFwe1
mFwe2
mFwe3
mFwe4
B
electroporate
with Fwe isoform
plasmid
Fwe KO astrocytes
Fwe win+ cells
(mFwe2 and mFwe4)
1:1 mixed
co-culture
Fwe lose+ cells
(mFwe1 and mFwe3)
Fix and image
after 24 h
to assess
cell death
C
Cell-Cell contact
Early apoptosis
Late apoptosis
mFwe win+
mFwe lose+
20 µm
CC3
DAPI
D
Win+Win
Lose+Lose
Win+Lose
Cell Viability %
Win+Win
Lose+Lose
Win+Lose
E
Apoptotic cells %
mFwe1
mFwe2
mFwe3
mFwe4
F
Cell-Cell contact
Early apoptosis
Late apoptosis
hFwe win+
hFwe lose+
20 µm
CC3
DAPI
G
Cell Viability %
Win+Win
Lose+Lose
Win+Lose
H
Apoptotic cells %
hFwe3
hFwe4

Figure 1

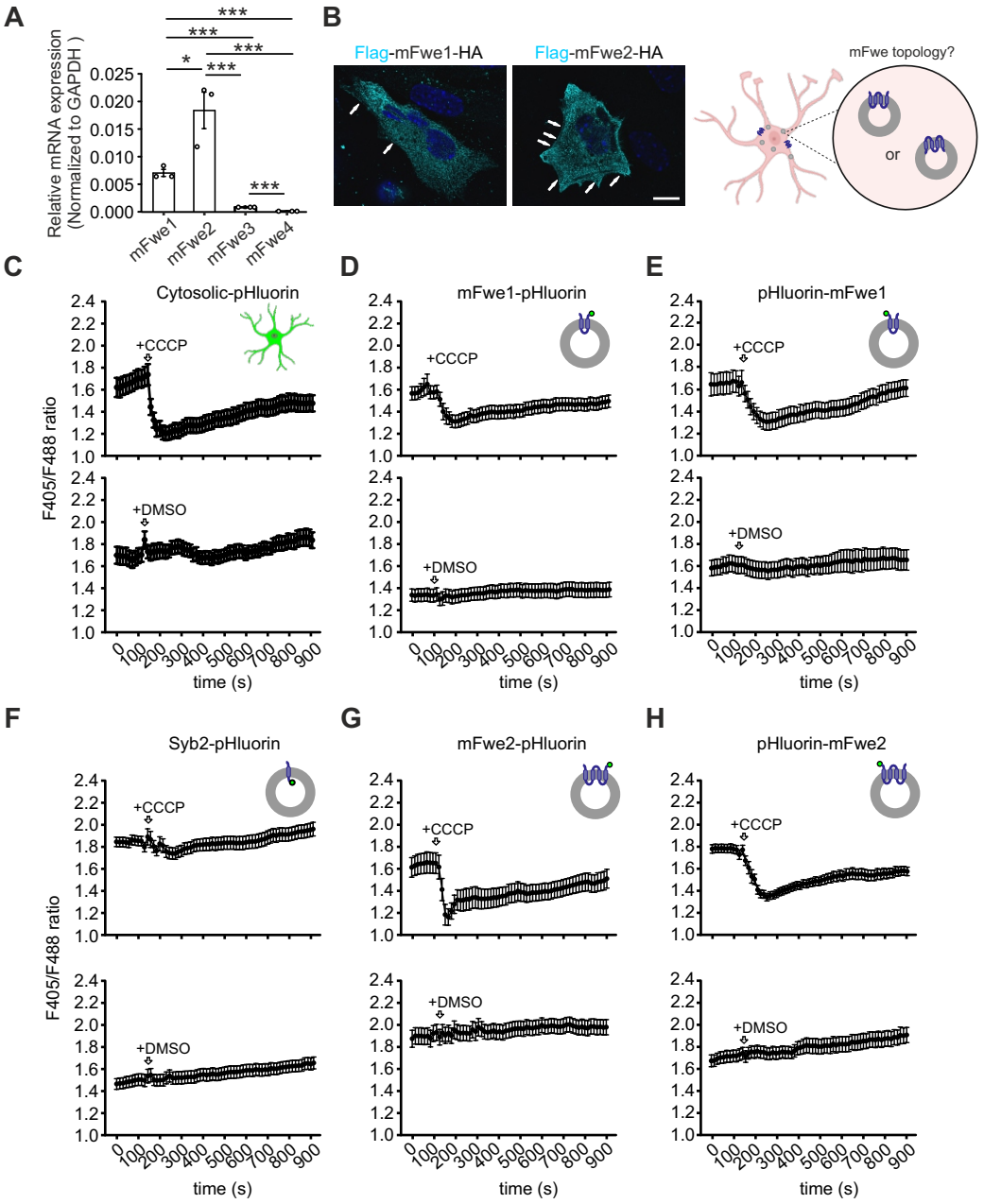
A
Relative mRNA expression (Normalized to GAPDH)
mFwe1
mFwe2
mFwe3
mFwe4
B
Flag-mFwe1-HA
Flag-mFwe2-HA
mFwe topology?
or
C
Cytosolic-pHluorin
D
mFwe1-pHluorin
E
pHluorin-mFwe1
F
Syb2-pHluorin
G
mFwe2-pHluorin
H
pHluorin-mFwe2
+CCCP
+DMSO
F405/F488 ratio
time (s)

Figure 2

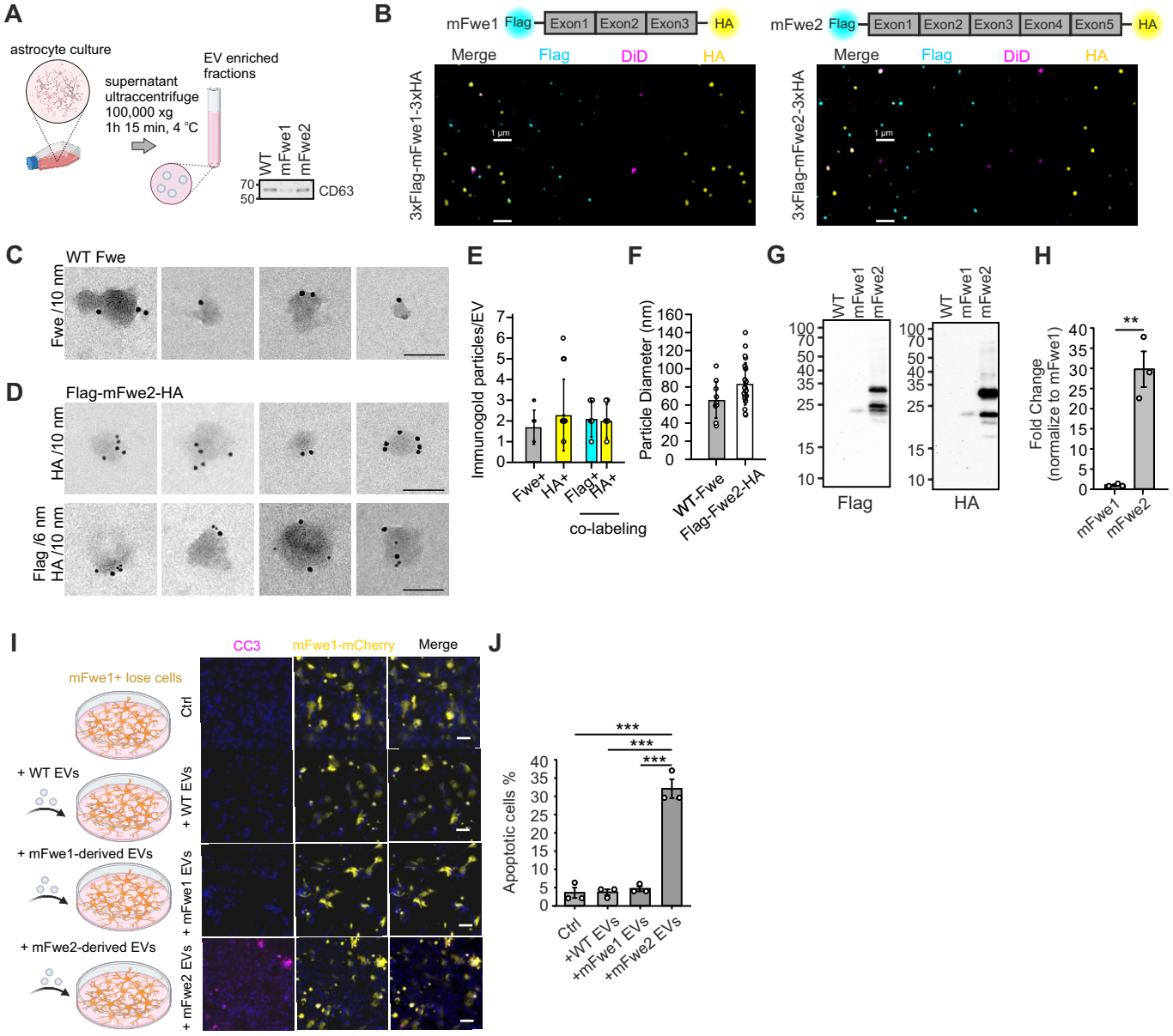
A
astrocyte culture
supernatant
ultraccentrifuge
100,000 xg
1h 15 min, 4 °C
EV enriched
fractions
WT
mFwe1
mFwe2
70
50
CD63
B
mFwe1
Flag
Exon1
Exon2
Exon3
HA
mFwe2
Exon4
Exon5
Merge
DiD
3xFlag-mFwe1-3xHA
3xFlag-mFwe2-3xHA
1 µm
C
WT Fwe
Fwe /10 nm
D
Flag-mFwe2-HA
HA /10 nm
Flag /6 nm
HA /10 nm
E
Immunogold particles/EV
Fwe+
HA+
Flag+
co-labeling
F
Particle Diameter (nm)
WT-Fwe
Flag-Fwe2-HA
G
Flag
H
Fold Change
(normalize to mFwe1)
**
I
CC3
mFwe1-mCherry
mFwe1+ lose cells
Ctrl
+ WT EVs
+ mFwe1-derived EVs
+ mFwe2-derived EVs
J
Apoptotic cells %
***
Ctrl
+WT EVs
+mFwe1 EVs
+mFwe2 EVs

Figure 3

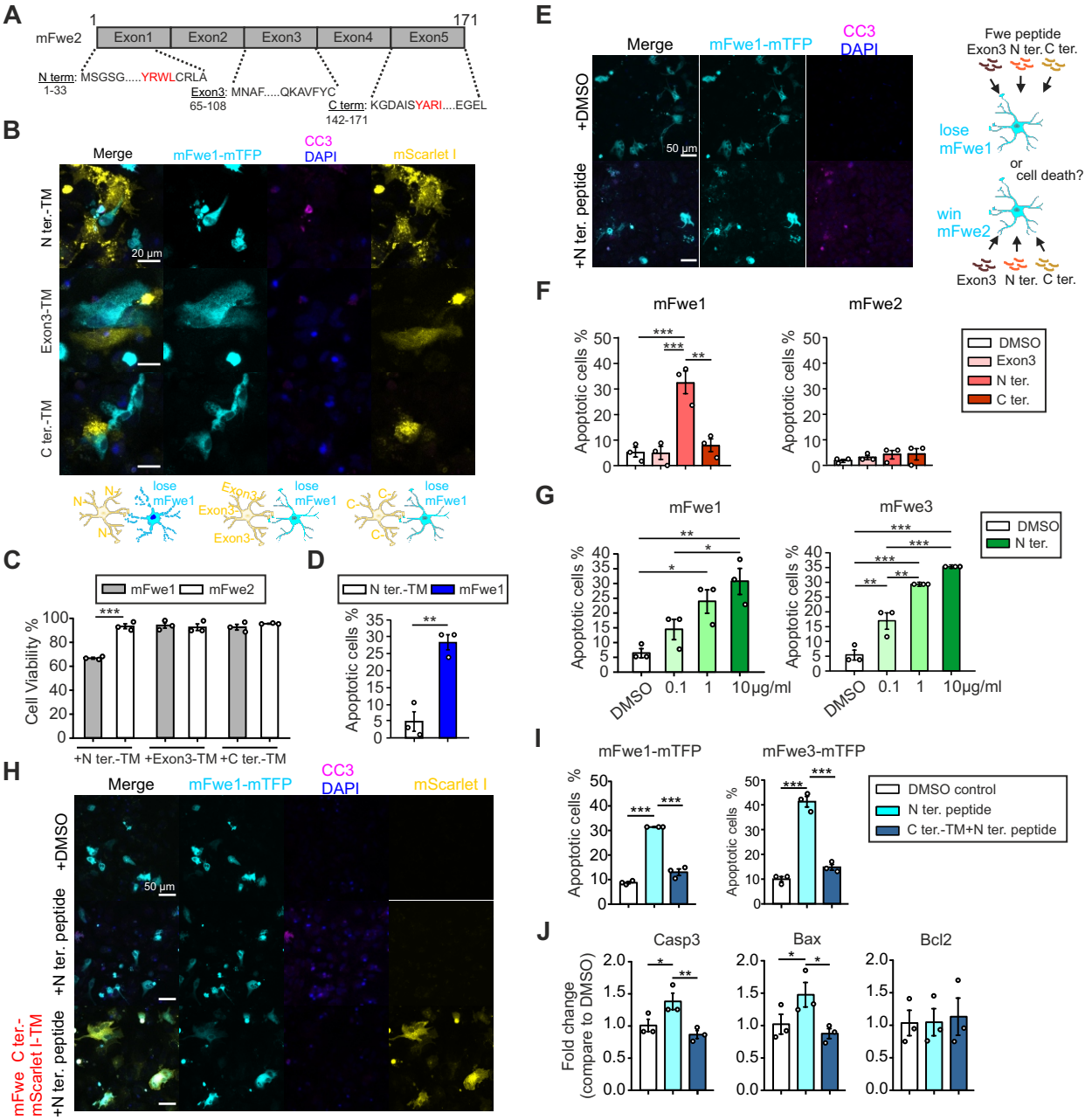
A
mFwe2
1
171
Exon1
Exon2
Exon3
Exon4
Exon5
N term: MSGSG.....YRWLCRLA
1-33
Exon3: MNAF.....QKAVFYC
65-108
C term: KGDAISYARI....EGEL
142-171
B
Merge
mFwe1-mTFP
CC3
DAPI
mScarlet I
N ter.-TM
Exon3-TM
C ter.-TM
20 µm
lose mFwe1
C
mFwe1
mFwe2
Cell Viability %
+N ter.-TM
+Exon3-TM
+C ter.-TM
D
N ter.-TM
mFwe1
Apoptotic cells %
E
Merge
mFwe1-mTFP
CC3
DAPI
+DMSO
+N ter. peptide
50 µm
Fwe peptide
Exon3 N ter. C ter.
lose mFwe1
or cell death?
win mFwe2
Exon3 N ter. C ter.
F
mFwe1
mFwe2
Apoptotic cells %
DMSO
Exon3
N ter.
C ter.
G
mFwe1
mFwe3
Apoptotic cells %
DMSO
N ter.
DMSO
0.1
1
10µg/ml
H
Merge
mFwe1-mTFP
CC3
DAPI
mScarlet I
+DMSO
+N ter. peptide
mFwe C ter.-mScarlet I-TM
+N ter. peptide
50 µm
I
mFwe1-mTFP
mFwe3-mTFP
Apoptotic cells %
DMSO control
N ter. peptide
C ter.-TM+N ter. peptide
J
Casp3
Bax
Bcl2
Fold change (compare to DMSO)

Figure 4

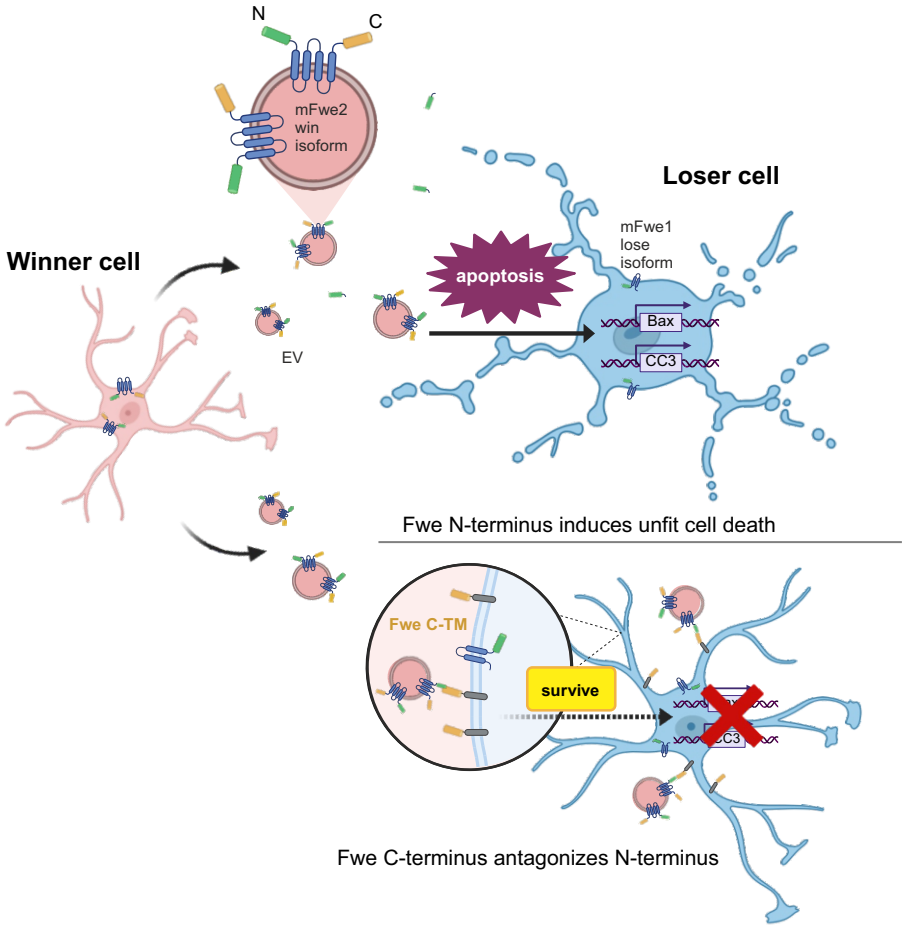
N
C
mFwe2
win
isoform
Winner cell
EV
Loser cell
mFwe1
lose
isoform
apoptosis
Bax
CC3
Fwe N-terminus induces unfit cell death
Fwe C-TM
survive
CC3
Fwe C-terminus antagonizes N-terminus

Figure 5

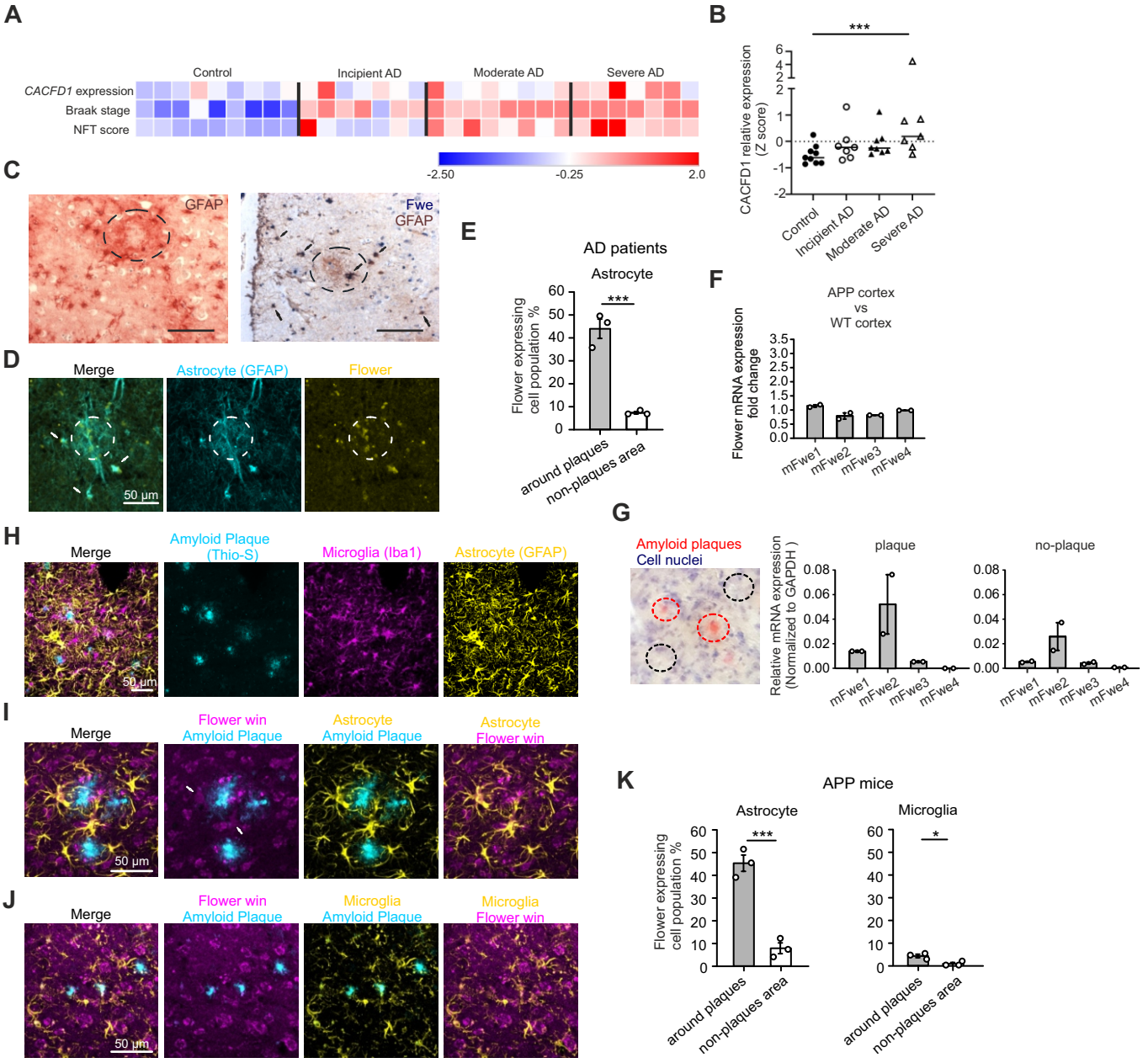
A
Control
Incipient AD
Moderate AD
Severe AD
CACFD1 expression
Braak stage
NFT score
-2.50
-0.25
2.0
B
***
CACFD1 relative expression (Z score)
Control
Incipient AD
Moderate AD
Severe AD
C
GFAP
Fwe
GFAP
D
Merge
Astrocyte (GFAP)
Flower
50 µm
E
AD patients
Astrocyte
***
Flower expressing cell population %
around plaques
non-plaques area
F
APP cortex
vs
WT cortex
Flower mRNA expression fold change
mFwe1
mFwe2
mFwe3
mFwe4
G
Amyloid plaques
Cell nuclei
plaque
no-plaque
Relative mRNA expression (Normalized to GAPDH)
H
Merge
Amyloid Plaque (Thio-S)
Microglia (Iba1)
Astrocyte (GFAP)
50 µm
I
Merge
Flower win
Amyloid Plaque
Astrocyte
Amyloid Plaque
Astrocyte
Flower win
50 µm
J
Merge
Flower win
Amyloid Plaque
Microglia
Amyloid Plaque
Microglia
Flower win
50 µm
K
APP mice
Astrocyte
Microglia
***
*
Flower expressing cell population %
around plaques
non-plaques area

Figure 6

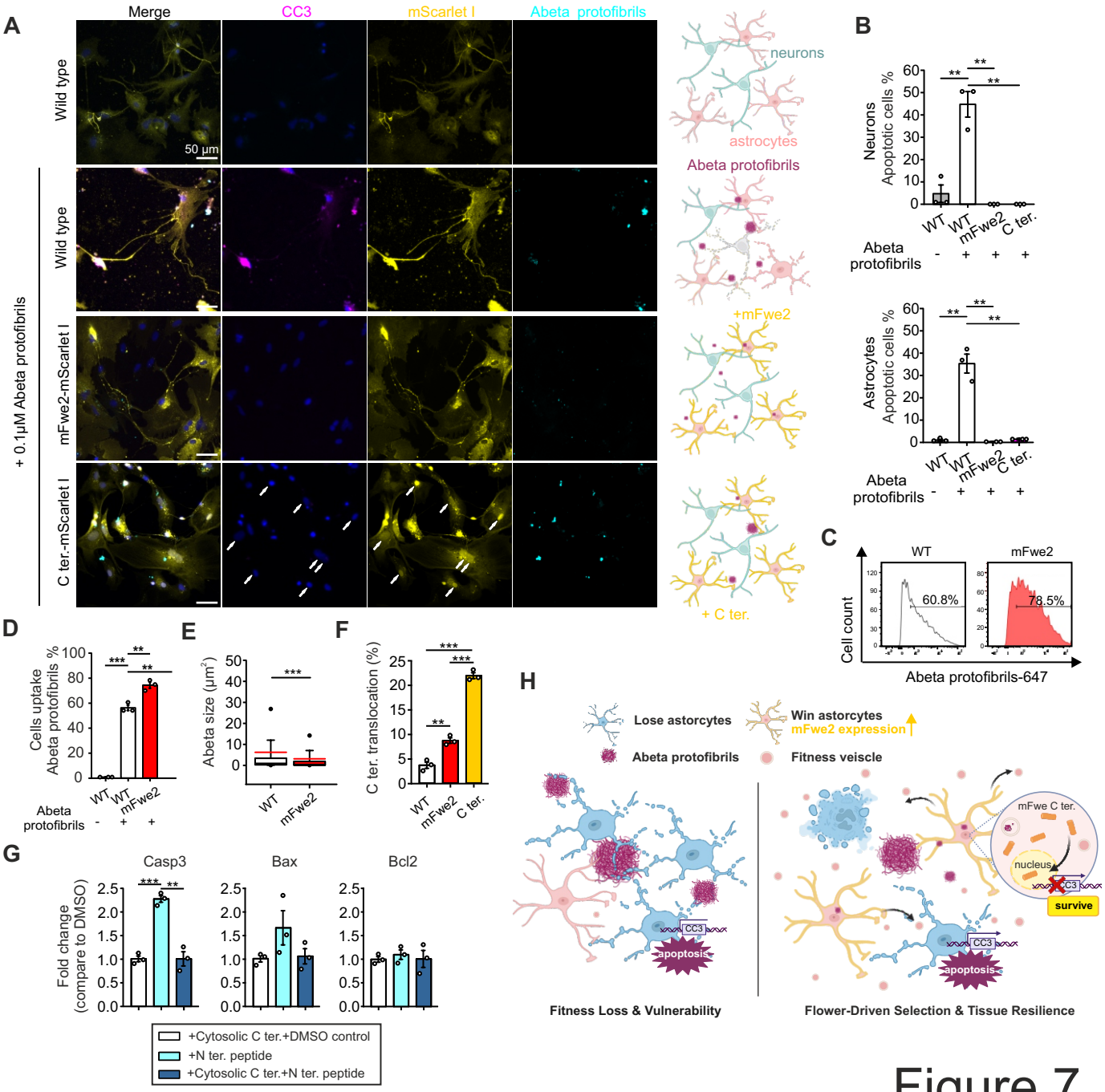
A
Merge
CC3
mScarlet I
Abeta protofibrils
Wild type
50 µm
Wild type
mFwe2-mScarlet I
C ter.-mScarlet I
+ 0.1µM Abeta protofibrils
neurons
astrocytes
Abeta protofibrils
+mFwe2
+ C ter.
B
Neurons
Apoptotic cells %
WT
WT
mFwe2
C ter.
Abeta protofibrils
Astrocytes
Apoptotic cells %
C
WT
mFwe2
60.8%
78.5%
Cell count
Abeta protofibrils-647
D
Cells uptake Abeta protofibrils %
Abeta protofibrils
E
Abeta size (µm²)
F
C ter. translocation (%)
G
Casp3
Bax
Bcl2
Fold change (compare to DMSO)
+Cytosolic C ter.+DMSO control
+N ter. peptide
+Cytosolic C ter.+N ter. peptide
H
Lose astorcytes
Win astorcytes
mFwe2 expression
Abeta protofibrils
Fitness veiscle
mFwe C ter.
nucleus
CC3
survive
apoptosis
Fitness Loss & Vulnerability
Flower-Driven Selection & Tissue Resilience

Figure 7

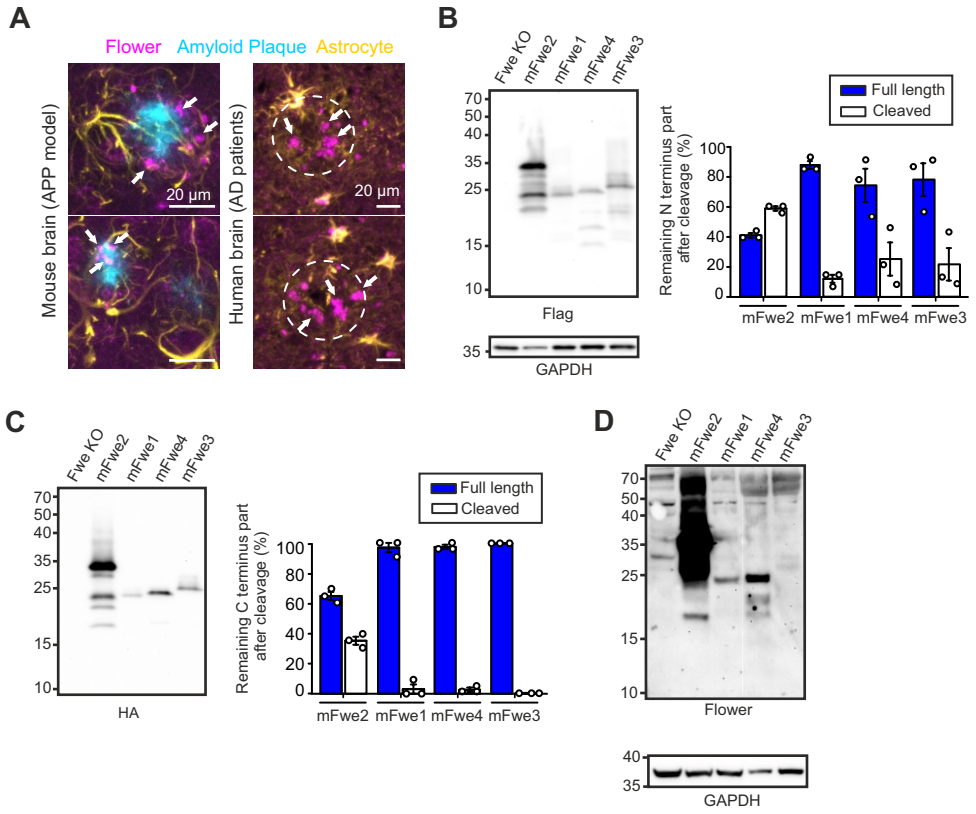
A
Flower
Amyloid Plaque
Astrocyte
Mouse brain (APP model)
Human brain (AD patients)
20 μm
20 μm
B
Fwe KO
mFwe2
mFwe1
mFwe4
mFwe3
70
50
40
35
25
15
10
Flag
35
GAPDH
Full length
Cleaved
Remaining N terminus part after cleavage (%)
100
80
60
40
20
0
mFwe2
mFwe1
mFwe4
mFwe3
C
Fwe KO
mFwe2
mFwe1
mFwe4
mFwe3
70
50
40
35
25
15
10
HA
Full length
Cleaved
Remaining C terminus part after cleavage (%)
100
80
60
40
20
0
mFwe2
mFwe1
mFwe4
mFwe3
D
Fwe KO
mFwe2
mFwe1
mFwe4
mFwe3
70
50
40
35
25
15
10
Flower
40
35
GAPDH

Figure EV1

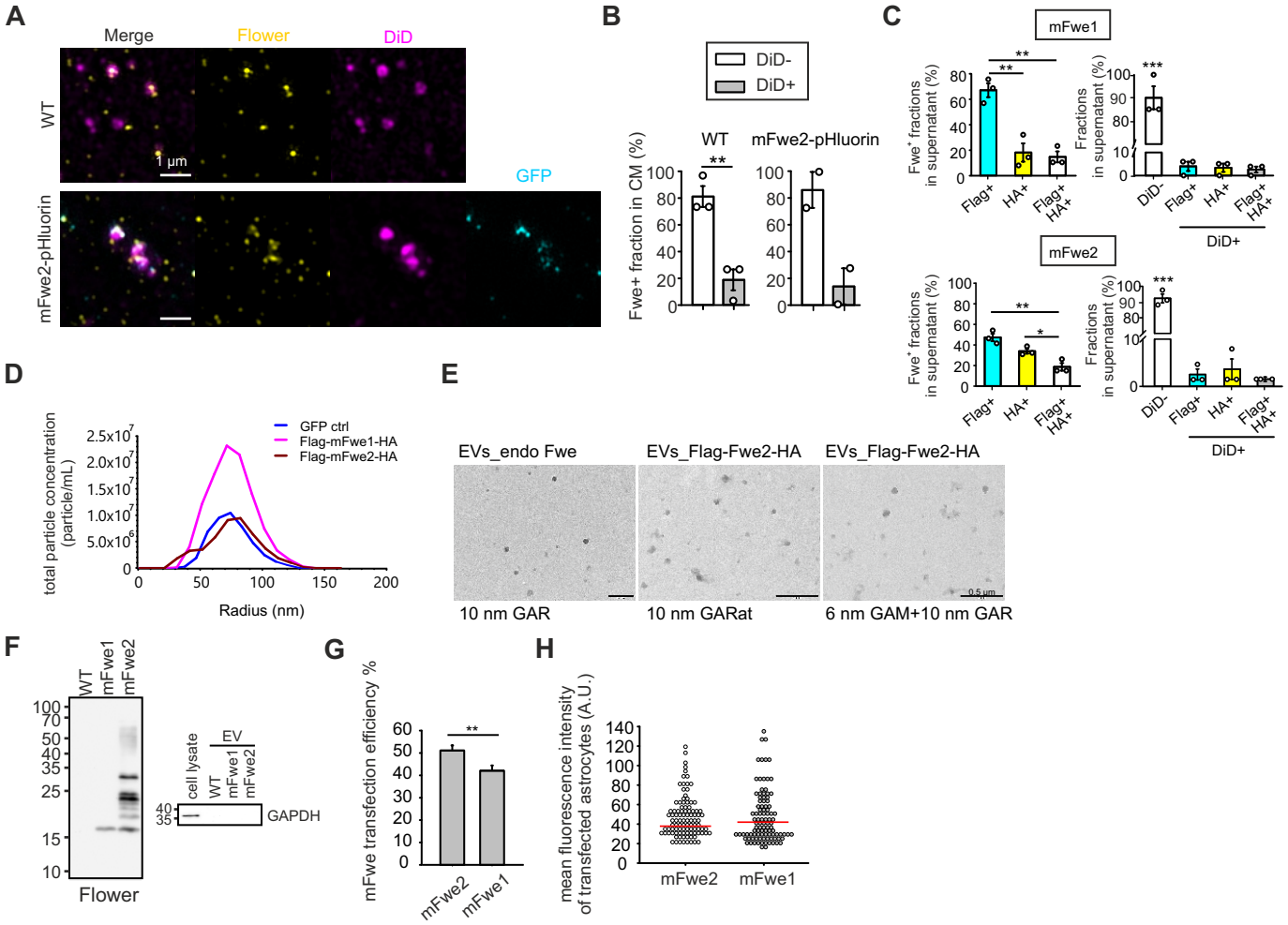
A
Merge
Flower
DiD
WT
1 µm
GFP
mFwe2-pHluorin
B
DiD-
DiD+
WT
mFwe2-pHluorin
Fwe+ fraction in CM (%)
C
mFwe1
Fwe+ fractions in supernatant (%)
Fractions in supernatant (%)
Flag+
HA+
Flag+ HA+
DiD-
DiD+
mFwe2
D
GFP ctrl
Flag-mFwe1-HA
Flag-mFwe2-HA
total particle concentration (particle/mL)
Radius (nm)
E
EVs_endo Fwe
EVs_Flag-Fwe2-HA
EVs_Flag-Fwe2-HA
10 nm GAR
10 nm GARat
6 nm GAM+10 nm GAR

F
WT
mFwe1
mFwe2
Flower
cell lysate
EV
GAPDH
G
mFwe transfection efficiency %
mFwe2
mFwe1
H
mean fluorescence intensity of transfected astrocytes (A.U.)
mFwe2
mFwe1

Figure EV2

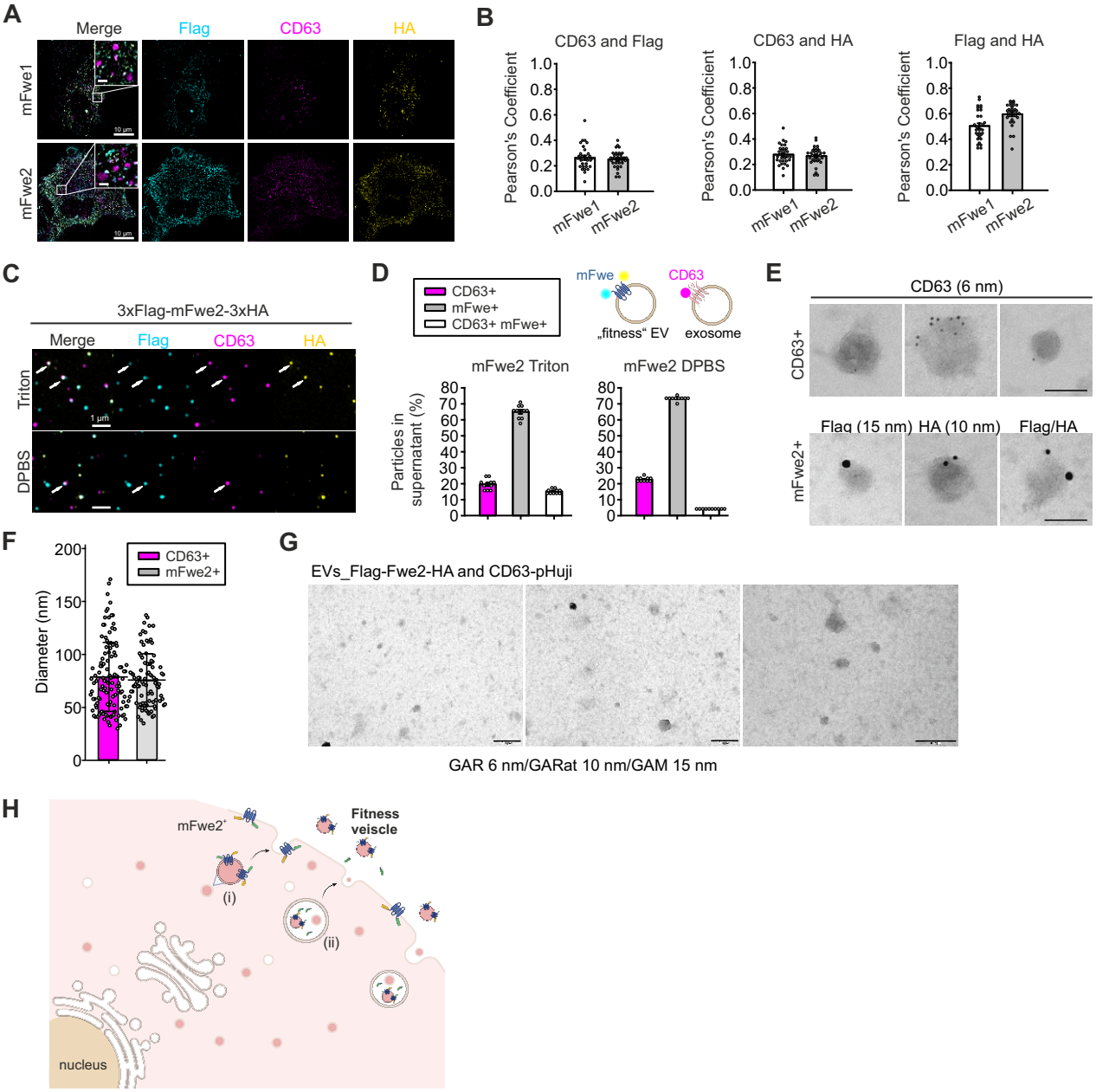
A
Merge
Flag
CD63
HA
mFwe1
mFwe2
B
CD63 and Flag
CD63 and HA
Flag and HA
Pearson's Coefficient
mFwe1
mFwe2
C
3xFlag-mFwe2-3xHA
Triton
DPBS
D
CD63+
mFwe+
CD63+ mFwe+
mFwe
CD63
„fitness" EV
exosome
mFwe2 Triton
mFwe2 DPBS
Particles in supernatant (%)
E
CD63 (6 nm)
CD63+
Flag (15 nm)
HA (10 nm)
Flag/HA
mFwe2+
F
CD63+
mFwe2+
Diameter (nm)
G
EVs_Flag-Fwe2-HA and CD63-pHuji
GAR 6 nm/GARat 10 nm/GAM 15 nm
H
mFwe2+
Fitness veiscle
(i)
(ii)
nucleus

Figure EV3

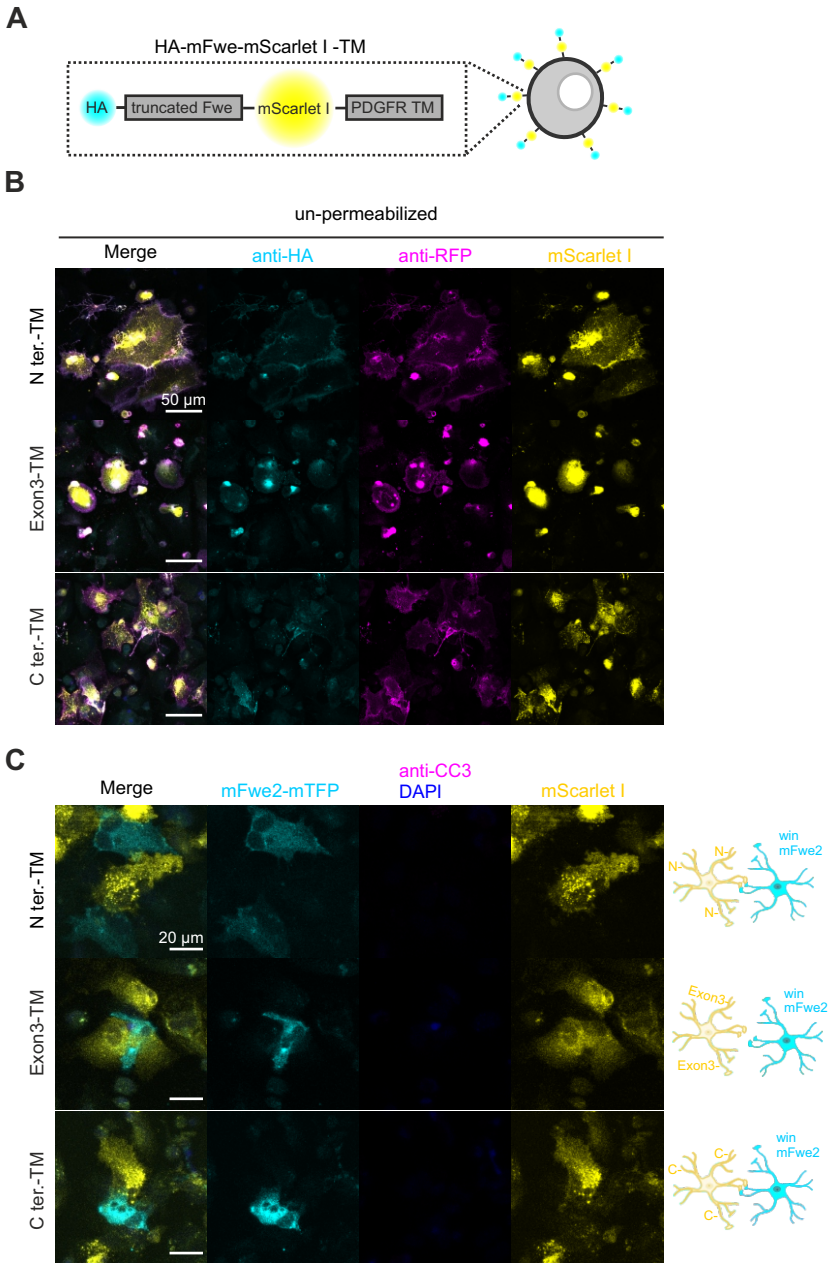
A
HA-mFwe-mScarlet I -TM
HA
truncated Fwe
mScarlet I
PDGFR TM
B
un-permeabilized
Merge
anti-HA
anti-RFP
mScarlet I
N ter.-TM
Exon3-TM
C ter.-TM
50 µm
C
Merge
mFwe2-mTFP
anti-CC3
DAPI
mScarlet I
N ter.-TM
Exon3-TM
C ter.-TM
20 µm
win
mFwe2
N-
Exon3-
C-

Figure EV4

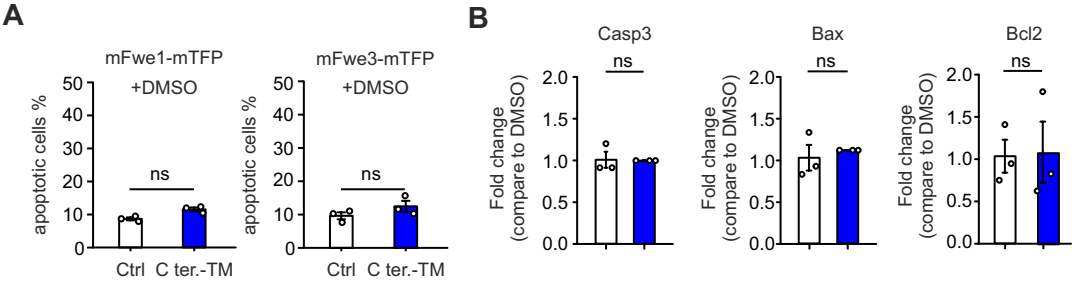
A
mFwe1-mTFP
+DMSO
apoptotic cells %
50
40
30
20
10
0
ns
Ctrl
C ter.-TM
mFwe3-mTFP
+DMSO
apoptotic cells %
50
40
30
20
10
0
ns
Ctrl
C ter.-TM
B
Casp3
ns
Fold change
(compare to DMSO)
2.0
1.5
1.0
0.5
0.0
Bax
ns
Fold change
(compare to DMSO)
2.0
1.5
1.0
0.5
0.0
Bcl2
ns
Fold change
(compare to DMSO)
2.0
1.5
1.0
0.5
0.0

Figure EV5

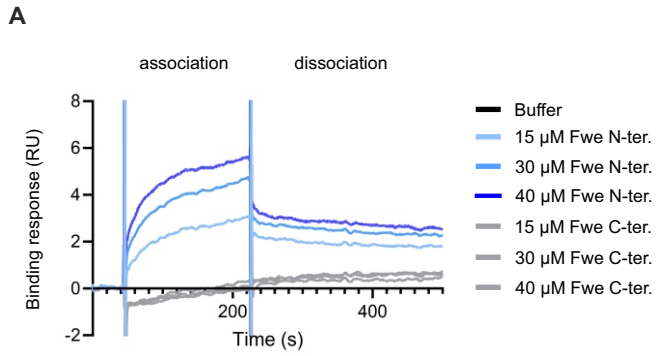
A
association
dissociation
Binding response (RU)
Time (s)
Buffer
15 µM Fwe N-ter.
30 µM Fwe N-ter.
40 µM Fwe N-ter.
15 µM Fwe C-ter.
30 µM Fwe C-ter.
40 µM Fwe C-ter.

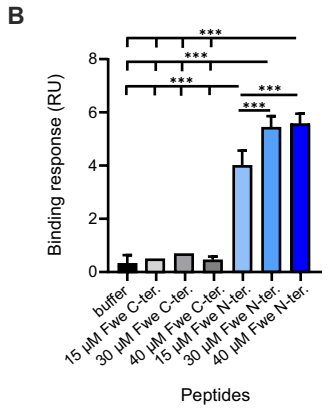
B
Binding response (RU)
buffer
15 µM Fwe C-ter.
30 µM Fwe C-ter.
40 µM Fwe C-ter.
15 µM Fwe N-ter.
30 µM Fwe N-ter.
40 µM Fwe N-ter.
Peptides

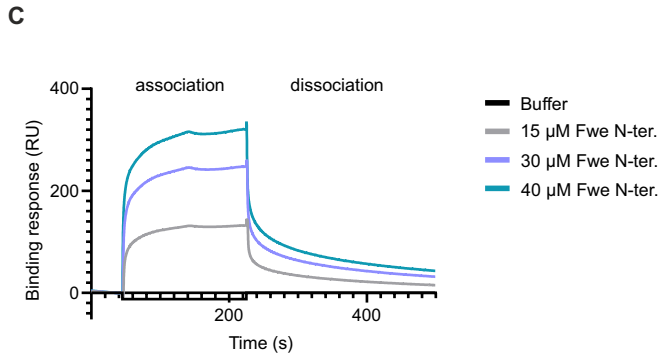
C
association
dissociation
Binding response (RU)
Time (s)
Buffer
15 µM Fwe N-ter.
30 µM Fwe N-ter.
40 µM Fwe N-ter.

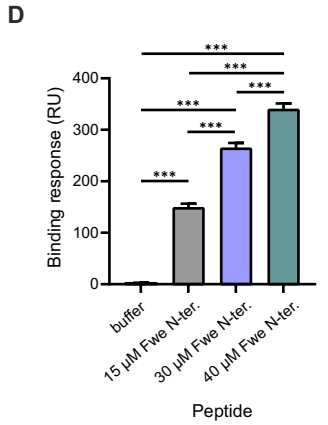
D
Binding response (RU)
buffer
15 µM Fwe N-ter.
30 µM Fwe N-ter.
40 µM Fwe N-ter.
Peptide

Figure EV6

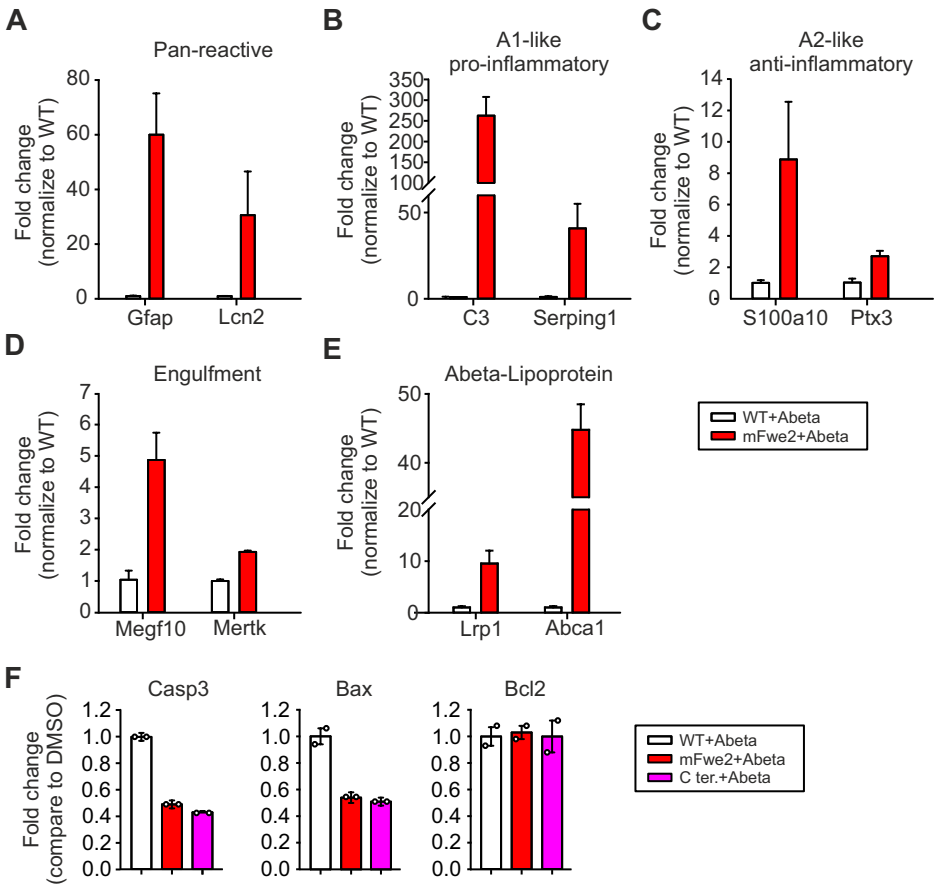
A
Pan-reactive
Fold change
(normalize to WT)
80
60
40
20
0
Gfap
Lcn2
B
A1-like
pro-inflammatory
Fold change
(normalize to WT)
350
300
250
200
150
100
50
0
C3
Serping1
C
A2-like
anti-inflammatory
Fold change
(normalize to WT)
14
12
10
8
6
4
2
0
S100a10
Ptx3
D
Engulfment
Fold change
(normalize to WT)
7
6
5
4
3
2
1
0
Megf10
Mertk
E
Abeta-Lipoprotein
Fold change
(normalize to WT)
50
40
20
10
0
Lrp1
Abca1
WT+Abeta
mFwe2+Abeta
F
Casp3
Bax
Bcl2
Fold change
(compare to DMSO)
1.2
1.0
0.8
0.6
0.4
0.2
0.0
WT+Abeta
mFwe2+Abeta
C ter.+Abeta

Figure EV7